Ocean Sci. Discuss., 12, 573–644, 2015
www.ocean-sci-discuss.net/12/573/2015/
doi:10.5194/osd-12-573-2015

Ocean Science
Discussions
Open Access

Carbon-based phytoplankton size classes retrieved via ocean color estimates of the particle size distribution

T. S. Kostadinov[1], S. Milutinović[2], I. Marinov[2], and A. Cabré[2]

[1]Department of Geography and the Environment, 28 Westhampton Way, University of Richmond, Richmond, VA 23173, USA
[2]Department of Earth and Environmental Science, Hayden Hall, University of Pennsylvania, 240 South 33rd St., Philadelphia, PA 19104, USA

Received: 12 March 2015 – Accepted: 15 April 2015 – Published: 6 May 2015

Correspondence to: T. S. Kostadinov (tkostadi@richmond.edu)

Published by Copernicus Publications on behalf of the European Geosciences Union.

Abstract

Owing to their important roles in biogeochemical cycles, phytoplankton functional types (PFTs) have been the aim of an increasing number of ocean color algorithms. Yet, none of the existing methods are based on phytoplankton carbon (C) biomass, which is a fundamental biogeochemical and ecological variable and the "unit of accounting" in Earth System models. We present a novel bio-optical algorithm to retrieve size-partitioned phytoplankton carbon from ocean color satellite data. The algorithm is based on existing algorithms to estimate particle volume from a power-law particle size distribution (PSD). Volume is converted to carbon concentrations using a compilation of allometric relationships. We quantify absolute and fractional biomass in three PFTs based on size – picophytoplankton (0.5–2 µm in diameter), nanophytoplankton (2–20 µm) and microphytoplankton (20–50 µm). The mean spatial distributions of total phytoplankton C biomass and individual PFTs, derived from global SeaWiFS monthly ocean color data, are consistent with current understanding of oceanic ecosystems, i.e. oligotrophic regions are characterized by low biomass and dominance of picoplankton, whereas eutrophic regions have large biomass to which nanoplankton and microplankton contribute relatively larger fractions. Global spatially integrated phytoplankton carbon biomass standing stock estimates using our PSD-based approach yield on average ~ 0.2–0.3 Gt of C, consistent with analogous estimates from two other ocean color algorithms, and several state-of-the-art Earth System models. However, the range of phytoplankton C biomass spatial variability globally is larger than estimated by any other models considered here, because the PSD-based algorithm is not a priori empirically constrained and introduces improvement over the assumptions of the other approaches. Satisfactory in situ closure observed between PSD and POC measurements lends support to the theoretical basis of the PSD-based algorithm. Uncertainty budget analyses indicate that absolute carbon concentration uncertainties are driven by the PSD parameter N_o which determines particle number concentration to first or-

OSD
12, 573–644, 2015

der, while uncertainties in PFTs' fractional contributions to total C biomass are mostly due to the allometric coefficients.

1 Introduction

Marine phytoplankton fix $\sim 50\,\mathrm{Gt\,C\,yr^{-1}}$, which accounts for about half of global net primary production (Field et al., 1998; Carr et al., 2006). Sinking organic matter powers the oceanic biological pump and enables long-term carbon sequestration that affects atmospheric carbon dioxide concentrations and thus climate (Eppley and Peterson, 1979; Falkowski et al., 1998; IPCC, 2013). Phytoplankton have different morphological (size and shape) and physiological (growth and mortality rates, response to nutrient, temperature and light conditions) characteristics that result in different biogeochemical roles – most importantly, sinking rates, but also silica drawdown, iron requirements, etc. They are grouped accordingly into phytoplankton functional types (PFTs, IOCCG 2014). Definitions of the PFTs can vary depending on the research goals and the operational methods used to quantify them (IOCCG, 2014). One of the primary distinguishing characteristics of the different PFTs is size (Vidussi et al., 2001; Le Quéré et al., 2005). Therefore size-based partitioning of phytoplankton can be used as a first-order proxy for many biogeochemical roles such as sinking, and a common operational definition of the PFTs is size-based. Thus the term phytoplankton size classes (PSCs) can be used as roughly equivalent to PFTs. Commonly, three PSCs are defined (Sieburth et al., 1978) – picophytoplankton ($< 2\,\mu m$ in diameter), nanophytoplankton (2–20 µm), and microphytoplankton ($> 20\,\mu m$), referred to as pico-, nano- and microplankton henceforth for brevity.

Global climate patterns can affect the spatio-temporal distribution of the PFTs by influencing light, nutrient, and temperature regimes (e.g., Marinov et al., 2013; Cabré et al., 2014), with potentially significant impacts on the oceanic food webs and C cycle. Phytoplankton themselves can influence climate via mechanisms such as the biological pump (e.g. Falkowski and Oliver, 2007), oceanic heating rates (e.g., Frouin and

OSD
12, 573–644, 2015

Iacobellis, 2002) and DMS production (e.g. Ayers and Cainey, 2007; Vallina and Simó, 2007). Therefore, important feedback loops related to oceanic ecosystems exist in the climate system. This necessitates the detailed characterization of oceanic ecosystems as a crucial component of the Earth system and the biosphere, i.e. an assessment of the spatio-temporal distribution, variability and future evolution of the PFTs (both stocks and production) globally and regionally. This can be accomplished using dynamic green ocean models as components of climate models that possess a realistic representation of the PFTs and predictive ability (e.g. Le Quéré et al., 2005; Hood et al., 2006).

Operational quantification of the PFTs on the required spatio-temporal scales can only be achieved via remote sensing. Since the late 1990's, ocean color remote sensing has provided a continuous global coverage of data that have greatly enhanced our understanding of the spatio-temporal characteristics of the oceanic ecosystems (e.g. McClain, 2009; Siegel et al., 2013). Remote-sensing reflectance as a function of wavelength, $R_{rs}(\lambda)$, quantifies ocean color and is the primary variable provided by ocean color sensors. Since the inception of ocean color remote sensing and bio-optical algorithm development, the canonical derived variable has been chlorophyll concentration (Chl) in surface waters, interpreted as a proxy for phytoplankton biomass. Chl can be estimated with classical empirical band-ratio algorithms (O'Reilly et al., 1998, 2000), or more sophisticated semi-analytical algorithms capable of retrieving several variables independently (Garver and Siegel, 1997; Maritorena et al., 2002). The latter have been motivated by the need to improve Chl retrievals by taking into account independently varying optically active constituents of the water column. Another important ecosystem variable, net primary productivity, is often parameterized as a function of Chl, among other variables (Behrenfeld and Falkowski, 1997a).

However, total Chl does not provide a full description of the state of the ecosystem, its history on a given time-scale, and its likely response to future forcing. Physiological acclimation to differing light levels can cause the ratio of Chl to carbon (C) to change, confounding interpretation of changes in Chl (Geider et al., 1987, 1998; Behrenfeld et al., 2005). It is carbon biomass in the living phytoplankton that is the variable of more

OSD
12, 573–644, 2015

direct relevance to the carbon cycle, other biogeochemical cycles, and climate. It is also the tracer variable most commonly used in biogeochemical routines of climate models (e.g. Gregg, 2008; Dunne et al., 2013). In addition, a more complete characterization of an oceanic ecosystem also necessitates partitioning of the carbon biomass into the different PFTs comprising the ecosystem. The Chl : C ratio itself can be used as a proxy for physiological status and an independent assessments of Chl and C allow the building of carbon-based productivity models (Behrenfeld et al., 2005; Westberry et al., 2008). It would be ideal to have independent and PFT-partitioned assessment of both Chl and C; this would allow partitioning of carbon-based productivity, improving upon existing class-specific estimates (Uitz et al., 2010).

The above considerations have led to recent developments in bio-optical modeling in two major directions, providing relevant remote-sensing products beyond Chl. First, multiple satellite ocean color algorithms for the estimation of various PFTs have been developed in the last decade (IOCCG, 2014). Some algorithms retrieve multiple PFT groups using differential absorption (Bracher et al., 2009) or second-order anomalies of the reflectance spectra (Alvain et al., 2008). Others (e.g. Brewin et al., 2010; Hirata et al., 2011; Uitz et al., 2006) are based on total (Chl) abundance and the ecological premise that smaller cells are associated with oligotrophic conditions whereas larger cells are associated with eutrophic conditions (Chisholm, 1992). Yet another class of algorithms relies on various spectral features, either absorption (Ciotti and Bricaud, 2006; Mouw and Yoder, 2010; Roy et al., 2013), or backscattering (Kostadinov et al., 2009, 2010) or both (Fujiwara et al., 2011). A summary of the available algorithms and their technical basis can be found in IOCCG (2014) and Hirata (2015). Of particular importance is that none of the existing algorithms retrieve C or base their PFT/PSC retrievals on total or fractional C content per PFT. Second, algorithms have been developed to retrieve particulate organic carbon (POC, e.g. Stramski et al., 2008 – henceforth, S08). However, these are empirical band-ratio algorithms the output of which is expected to be tightly correlated to Chl, which is derived in much the same way.

OSD
12, 573–644, 2015

The retrieval of just the living phytoplankton carbon concentration represents significant progress (Behrenfeld et al., 2005 – henceforth, B05), but it is much harder to measure reliably remotely and even in-situ (Menden-Deuer and Lessard, 2000; Graff et al., 2012). The B05 method is a first order assessment using a direct empirical scaling of the backscattering coefficient to estimate phytoplankton C by multiplying the particulate backscattering at 440 nm ($b_{bp}(440)$) by 13 000 mg C m^{-2} to convert it to phytoplankton carbon (after a background subtraction). This constant does not change in time or space and is picked so that reasonable Chl : C and POC : living C values are achieved. Their approach does not take into account the effects of variable particle size distributions on this scaling factor. Even if particle composition is assumed to be roughly constant and corresponding to predominantly living phytoplankton cells, changes in their particle size distribution will change the backscattering per unit C biomass due to different scattering efficiencies exhibited by particles of different size (this can be quantified by Mie theory, e.g. Stramski and Kiefer, 1991; Kostadinov et al., 2009).

Significant advances have been made in estimating biovolume in-situ (Moberg and Sosik, 2012). Recent advances also allow for the quantification of an assumed power-law particle size distribution from space and the estimation of particulate volume in any size class from ocean color satellite data (Kostadinov et al., 2009, 2010). Henceforth, Kostadinov et al. (2009) is referred to as KSM09, and the PSD algorithm as the KSM09 algorithm. Here, we leverage the KSM09 algorithm and an existing compilation of allometric relationships that link cellular C content to cellular volume (Menden-Deuer and Lessard, 2000, henceforth – MDL2000), in order to *(1) estimate total C biomass using the power-law PSD parameters as input and (2) recast the volume-based PSCs of the* KSM09 *algorithm in terms of C biomass.* The effects of variable PSD have been taken into account for the first time, relaxing the assumption of a constant backscattering to carbon relationship. Importantly, to our knowledge this is the first attempt to provide size class partitioning of phytoplankton C biomass from space. We first present the methodology and apply the algorithm to SeaWiFS global monthly reflectance data, focusing on climatological patterns and comparison with existing phytoplankton carbon estimates

OSD
12, 573–644, 2015

and Earth System model results. We then assess global mixed layer phytoplankton biomass stock and compare to existing estimates. Importantly, we quantify partial uncertainties on a per-pixel basis by propagating existing input parameter uncertainties (when quantifiable and available) to the C-based products.

2 Data and methods

2.1 Estimation of carbon biomass using PSD retrievals

2.1.1 Step 1: Retrieval of suspended particulate volume from ocean color remote sensing data

We first quantify the volume concentration of suspended particulate matter from ocean color data by applying the KSM09 algorithm to estimate the parameters of an assumed power-law particle size distribution. These parameters are retrieved using look-up tables (LUTs) constructed using Mie theory of scattering (Mie, 1908). The LUTs relate the spectral shape and magnitude of the particulate backscattering coefficient at blue-green wavelengths ($b_{bp}(\lambda)$ [m^{-1}]) to the power-law slope ξ [unitless] of the PSD and the differential number concentration of suspended particles at a reference diameter (here, 2 µm), N_o [m^{-4}] (Junge, 1963; Boss et al., 2001; KSM09):

$$N(D) = N_o \left(\frac{D}{D_o} \right)^{-\xi} \quad (1)$$

In Eq. (1), D [m] is the equivalent spherical diameter (ESD) (Jennings and Parslow, 1988).

Equation (1) can be integrated over a chosen size range in order to derive the total number, area or volume concentration of the particles in that range. Volume concentration [m^3 of particles $(m^3$ seawater$)^{-1}$] can thus be computed as (Kostadinov et al.,

OSD
12, 573–644, 2015

2010):

$$V = \int_{D_{\min}}^{D_{\max}} \left(\frac{\pi D^3}{6}\right) N_o \left(\frac{D}{D_o}\right)^{-\xi} \mathrm{d}D \quad (2)$$

Even though the power-law PSD is considered a simple two-parameter model, in reality it is a four-parameter parameterization, because in practical applications the upper and lower limits of integrals such as Eq. (2) need to be known (Boss et al., 2001). Assuming biogenic origin of scattering particles, Kostadinov et al. (2010) developed a novel method of estimating three phytoplankton size classes (PSCs), defining each class as its fractional contribution to total biovolume.

2.1.2 Step 2: Retrieval of size-partitioned absolute and fractional phytoplankton carbon biomass

Estimation of carbon concentration follows the methodology first outlined in Kostadinov (2009). The volume-to-carbon allometric relationships compiled by MDL2000 are used to quantify POC by converting the volume estimates of Eq. (2) to C concentration. The relationships in MDL2000 have the general form:

$$C_{\mathrm{cell}} = aV_{\mathrm{cell}}^{b} \quad (3)$$

where C_{cell} is cellular carbon content [pg C cell^{-1}], a and b are group-specific constants and V_{cell} is cell volume [µm^3]. Incorporating the allometric relationship of Eq. (3) into Eq. (2) yields an estimate of particulate carbon mass concentration (i.e. POC) in a given size range, $D_{\min}$ to $D_{\max}$. The carbon biomass of living phytoplankton only (C, [mg m^{-3}]) can then be estimated by multiplication by 1/3:

$$C = \frac{1}{3} \int_{D_{\min}}^{D_{\max}} 10^{-9} a \left(\frac{10^{18}\pi D^3}{6}\right)^{b} N_o \left(\frac{D}{D_o}\right)^{-\xi} \mathrm{d}D \quad (4)$$

OSD
12, 573–644, 2015

The factor of 1/3 is used because it is approximately in the middle of the published range for the phytoplankton C : POC ratio in ocean regions of variable trophic status (0.14 to 0.49) (B05; DuRand et al., 2001; Eppley et al., 1992; Gundersen et al., 2001; Oubelkheir et al., 2005). The factors 10^{-9} and 10^{18} are applied in Eq. (4) for conversion from pg (Eq. 3) to mg of C and from m^3 to μm^3, respectively.

The formulation of Eq. (4) allows phytoplankton carbon biomass to be estimated for any size range. Here, we partition the biomass in three classical phytoplankton size classes (PSCs, Sieburth et al., 1978): picoplankton ($0.5\,\mu m \le D \le 2\,\mu m$), nanoplankton ($2\,\mu m \le D \le 20\,\mu m$) and microplankton ($20\,\mu m \le D \le 50\,\mu m$). There is some variation in the literature regarding the cut-off values that are used in definition of these categories, because they are rather arbitrary. The only objective cut-off value is that for the minimum autotrophic picoplankton size (0.5 µm), as this is the reported ESD of the smallest known marine photosynthesizer (Partensky et al., 1999). The maximum size threshold for unicellular phytoplankton is not as clear and we settle on 50 µm, since larger algal cells are seldom encountered even in eutrophic conditions (Charles Stock, personal communication, 2013) and are particularly rare in the open ocean (Roy et al., 2013).

The parameters *a* and *b* in Eq. (5), pertaining to the groups of phytoplankton that are relevant for this study, are selected from MDL2000 and are presented in Table 1a. C biomass is estimated using more than one allometric relationship in order to achieve a global optimal solution. The biomass of picoplankton is computed by implementing the parameters for cells with volume below $3000\,\mu m^3$ ($D < 17.894\,\mu m$) in Eq. (4) for *D* from 0.5 to 2 µm. Nanoplankton biomass is computed by combining all the three sets of *a* and *b* values listed in Table 1. The first set (same as for picoplankton) is used in Eq. (4) for *D* between 2 and 17.894 µm. The second (for generic non-diatomaceous phytoplankton) and third set (for diatoms above $3000\,\mu m^3$) are applied separately in Eq. (4) for *D* between 17.894 and 20 µm and the results are averaged and added to the result of applying the first set of parameters, obtaining the overall nanoplankton biomass. Similarly, microplankton biomass is determined as the arithmetic mean of the respective output of Eq. (4) when the second and the third sets of *a* and *b* values

OSD
12, 573–644, 2015

are used for D from 20 to 50 µm. The biomass of the entire phytoplankton community (0.5 µm ≤ D ≤ 50 µm) is the sum of the respective biomass values for the three PSCs.

Analytical solution of the integral of Eq. (4) thus results in the following expression for a given size class:

$$C = \sum_{i=1}^{p} w_i \frac{1}{3} 10^{-9} a_i \left(\frac{10^{18}\pi}{6}\right)^{b_i} N_o D_o^{\xi} \frac{1}{3b_i - \xi + 1} \left(D_{\max i}^{3b_i-\xi+1} - D_{\min i}^{3b_i-\xi+1}\right) \quad (5)$$

In the above equation, p represents the number of distinct sets of allometric coefficients used, i.e. $p = 3$ for total carbon and nanoplankton, $p = 1$ for picoplankton, and $p = 2$ for microplankton. Table 1b lists the weights w_i applied for each allometric relationship. The $D_{\max}$ and $D_{\min}$ values are selected as appropriate from the size ranges of the size class or the limits of applicability of the ith allometric relationship (Table 1b). Equation (5) is not valid when the denominator is exactly 0. In the very few cases when this happens operationally to within machine precision, the value of the PSD slope is nudged by a very small value (much smaller than its uncertainty).

Finally, the three PSCs are expressed as relative fractions of total phytoplankton C biomass, by dividing the PSC's biomass by total biomass. This expression of the PSCs is a recast of the volume-fraction based PSCs of KSM09 in terms of carbon biomass, which represents a significant improvement since carbon biomass because C biomass is an important component of the global carbon cycle and is thus linked to climate. These C-based PSCs are also more directly comparable to variables in Earth System models. As such they are of direct interest to the modeling community, which is intended as a primary user of the novel PSC products.

2.2 Input ocean color satellite data

Global mapped monthly composites of remote sensing reflectance $R_{rs}(\lambda)$ [sr^{-1}] nominally at 412, 443, 490, 510, and 555 nm, measured by the Sea-viewing Wide Field-of-view Sensor (SeaWiFS) (reprocessing R2010.0) were downloaded from the NASA

OSD
12, 573–644, 2015

Ocean Biology Processing Group (OBPG) archive at (http://oceandata.sci.gsfc.nasa.gov/SeaWiFS/Mapped/Monthly/9km/Rrs/). The data have a nominal resolution of ~ 9 km and are mapped to an equidistant cylindrical projection. Measurements were available for the period September 1997 to December 2010, with the exception of a few months after 2007, when technical problems occurred (namely, February, March of 2008 and May of 2009 are missing data months, while January and July 2008 and September and October 2009 exhibit very sparse data).

The monthly $R_{rs}(\lambda)$ maps were used to retrieve the spectral particulate backscattering coefficient ($b_{bp}(\lambda)$, [m^{-1}], λ same as for the input reflectances), using the algorithm of Loisel and Stramski (2000) and Loisel et al. (2006) (henceforth – the LAS2006 algorithm), with a solar zenith angle (SZA) of 0° because the input $R_{rs}(\lambda)$ are fully normalized. The spectral slope of $b_{bp}(\lambda)$, η, was calculated using a linear regression on the log-transformed data at the 490, 510 and 555 nm bands. The KSM09 algorithm (Sect. 2.1.1) was then applied to η and b_{bp} at 443 nm in order to obtain the PSD parameters ξ and N_o, which were subsequently used in Eq. (5) to obtain monthly 9 km maps of total and PSC-partitioned absolute and fractional C biomass.

2.3 Phytoplankton carbon estimates from Earth System Models

Phytoplankton carbon was also derived from the output of a group of Earth System simulations from the recent Coupled Model Intercomparison Project CMIP5 (Taylor et al., 2012). CMIP5 model output was downloaded from http://pcmdi9.llnl.gov/esgf-web-fe/. The models and their basic characteristics are summarized in Table 2. The marine biogeochemical routine for models CanESM2 and MRI-ESM1 is based on the basic NPZD (Nutrient Phytoplankton Zooplankton Detritus) structure with only one phytoplankton type and one nutrient (nitrate). The complexity increases with MPI-ESM, NorESM1, HadGEM2, and GISS-E2 via inclusion of more nutrients (nitrate, silicate, iron) and additional types of phytoplankton for HadGEM2 and GISS-E2. Finally, IPSL-CM5, GFDL-ESM2, and CESM1-BGC are the most ecologically complex models, with at least 2

OSD
12, 573–644, 2015

types of phytoplankton, zooplankton types, more than 20 biogeochemical tracers, and inclusion of ballast in the last two models.

We derive the ensemble mean phytoplankton C from 21 years of "present" historical output (1990 to 2010) of the variable "phyc" ("total phytoplankton carbon concentration"). Molar concentration provided by the models (mol C m^{-3}) was converted to mass concentration (mg C m^{-3}) using the atomic weight of carbon (12.011 g mol^{-1}, Wieser et al., 2013). The "present" output is mostly based on the historical scenario (years 1850 to 2005) forced by observed atmospheric changes (both anthropogenic and natural). The last five years (2006 to 2010) of the "present" output are based on the RCP8.5 scenario. We selected 14 models with different resolutions (ocean grid varies from 0.5 to 2°) and complexities in their biogeochemical and ecological modules, as described in Table 2. All model output was resampled to a 1° grid before calculating first the temporal average of each model individually, and then averaging each model's climatology to obtain the ensemble mean model climatology. Because of significant similarities between model pairs (Cabré et al., 2014), when computing ensemble averages we used weights as in Table 2. Before computing averages, biomass values below 0 were set to missing data, and in the case of the MRI-ESM1 model values below 0.01 mg m^{-3} C were also set to missing values. Those occur primarily along the coasts and are considered a numerical artifact (most are $\sim 10^{-18}$ mg m^{-3} C in areas where biomass is expected to be high).

2.4 In-situ POC-PSD closure analysis

In-situ closure (i.e. agreement) between POC and PSD data was investigated as a validation of the allometric methodology presented here. Nearly coincident observations of both PSD (Coulter Counter measurements) and POC (analytical chemical determinations) from Atlantic Meridional Transect (AMT) cruises 2, 3 and 4, conducted in 1996 and 1997, were obtained from the British Oceanographic Data Centre (BODC, http://www.bodc.ac.uk/). The 2–20 µm diameter range of the PSD data was used to fit a regression line on the log10-transformed, bin-width normalized data, yielding es-

OSD
12, 573–644, 2015

timates of the PSD parameters, ξ and N_o. These were used as inputs to Eq. (5) to estimate allometric phytoplankton C from the PSD data. Chemical POC data were provided in units of $\mu mol\,L^{-1}$, which were converted to $mg\,m^{-3}$ using carbon's atomic weight of $12.011\,g\,mol^{-1}$ (Wieser et al., 2013). Phytoplankton C was then estimated from POC by multiplication by 1/3. Match-ups were then constructed between the two methods of estimating phytoplankton carbon concentration, considering two data points a valid match-up only if they were closer than 4.24 km from each other (diagonal of a 3 km × 3 km box), samples were taken within 3 h of each other, and within 15 m vertical separation. Using these criteria 44 match-ups were obtained.

2.5 Propagation of uncertainty to carbon products and composite imagery

The proximal input parameters of the absolute and fractional C-based PSC algorithm are the PSD slope ξ, the N_o parameter, and up to six allometric coefficients (Table 1a and b). Uncertainties (in terms of standard deviation) in these input parameters are propagated to the algorithm products on a per-pixel basis. The uncertainty of absolute or fractional carbon concentration, C, in any size class is estimated as

$$\sigma_C = \sqrt{\left(\frac{\partial C}{\partial \xi}\right)^2 \sigma_\xi^2 + \left(\frac{\partial C}{\partial N_o}\right)^2 \sigma_{N_o}^2 + \sum_{i=1}^{p} \left(\frac{\partial C}{\partial a_i}\right)^2 \sigma_{a_i}^2 + \sum_{i=1}^{p} \left(\frac{\partial C}{\partial b_i}\right)^2 \sigma_{b_i}^2} \quad (6)$$

This is the standard analytical approximation of error propagation formulation (e.g. Ku, 1966). The partial derivatives of C with respect to the input parameters are calculated analytically from Eq. (5), where $p = 1$, 2 or 3 depending on the size class (Table 1a and b, Sect. 2.1.2). The KSM09 algorithm provides standard deviations of the output PSD parameters as a quantification of partial uncertainty. The MDL2000 allometric coefficients are derived from linear regressions and their 95 % confidence intervals are provided. These were converted to standard deviations by dividing by the respective cumulative t distribution value for each case (Table 1 and MDL2000, their Table 4).

OSD
12, 573–644, 2015

The estimate in Eq. (6) represents only a part of the uncertainty in C, because only parts of the PSD parameters' uncertainties are quantifiable and provided by KSM09. Unquantified sources of error are discussed qualitatively in Sect. 3.7.3.

Monthly and overall mission composite imagery was computed from the respective monthly maps of Chl and the carbon-based products as the arithmetic mean (in linear space) of all available data for a given pixel. Uncertainties of the composite imagery data were determined as

$$\sigma_{\text{composite}} = \frac{\sqrt{\sum_{k=1}^{N} \sigma_k^2}}{N} \tag{7}$$

where σ_k is the standard deviation of the kth term of the composite average, out of a total of N terms. It is evident from Eq. (7) that when N increases, random, zero-centered uncertainties will generally decrease unless a data point of very large uncertainty participates in the sum. Note that systematic bias (e.g. a consistent underestimate) cannot be quantified or reduced in this way.

2.6 Algorithm output analyses and ancillary data

In order to investigate relationships of the novel C-based products with Chl concentration, monthly mapped SeaWiFS 9 km OC4v6 Chl [mg m^{-3}] (O'Reilly et al., 2000), was obtained from NASA OBPG (reprocessing R2010.0) The mission composite was also obtained in order to study climatological relationships. The mission composite Chl image was downsampled to 1° resolution using 2-D convolution and the 0.08 mg m^{-3} isoline of Chl was extracted in order to delineate the subtropical gyres on maps. For comparison purposes, phytoplankton C biomass was also estimated using the B05 method with the same LAS2006-derived $b_{\text{bp}}(443)$ as used in the PSD-based algorithm. POC was retrieved using the S08 algorithms (using the $R_{\text{rs}}(490)/R_{\text{rs}}(555)$ band ratio parameterized with all data, see their Table 2). The same R2010.0 SeaWiFS re-

OSD
12, 573–644, 2015

flectances were used as for our algorithm. The POC retrievals were multiplied by 1/3 to approximate the living fraction.

The assumptions of the C biomass algorithm are more likely to be violated in shallow coastal regions, where non-biogenic particles may contribute to backscattering significantly (e.g. Toole et al., 2001; Otero and Siegel., 2004). We thus excluded the continental shelves from some analyses as indicated. The shelves were identified as areas shallower than 200 m and determined using the bathymetry data from the NOAA/NGDC ETOPO1 data set (Amante and Eakins, 2009), downsampled to 9 km or 1° resolutions as needed. In order to display the coastline on maps, the L1 layer of the GSHHG v2.2.3 (Wessel and Smith, 1996) coastline data set was extracted with the NOAA/NGDC GEODAS-NG software.

In order to estimate global phytoplankton C biomass standing stock within the mixed layer, monthly mixed layer depth (MLD) for the 1997–2010 SeaWiFS mission period was computed from the UK Met Office Hadley Centre's monthly global objective analyses fields of seawater potential temperature and salinity (version EN3_v2a) (Ingleby and Huddleston, 2007). The fields were provided on a regular grid of 1° longitude/latitude resolution and 42 unequally spaced depth levels. For each grid cell and depth, seawater density was computed using the equation of state of seawater (UNESCO et al., 1980). Linear interpolation was then applied to every respective vertical profile of temperature and density to compute MLD, using the threshold approach of de Boyer Montégut et al. (2004) (±0.2 °C or 0.03 kg m^{-3}). Following their recommendation, the shallower of the temperature- and density-based values was chosen as the best estimate of MLD. Monthly and overall SeaWiFS-era global MLD composites were computed from the resulting MLD maps using the median of all available MLD values in a particular grid cell. We selected the median because it is a more representative measure of central tendency for MLD than the mean, as was shown by de Boyer Montégut et al. (2004).

Global phytoplankton C biomass stock was computed from the monthly and overall mission composites that were first downsampled from 9 km to 1° resolution in log10

OSD
12, 573–644, 2015

space using a 2-D convolution kernel of size 12 × 12. Using composites and downsampling them is a spatio-temporal gap filling technique as it reduces or eliminates data gaps that would bias the global estimate. Since ocean color data are not vertically resolved, we assume that the vertical profile of phytoplankton C biomass is uniform down to the mixed layer depth (MLD). Thus biomass stock was computed by multiplying surface satellite estimates of C biomass by the corresponding MLD value, and all valid pixels were summed after also multiplying by the pixel area. Pixel area was approximated using the area integral on a spherical Earth. Biomass stock was computed for the entire ocean as well the open ocean, excluding the shelves.

3 Results and discussion

3.1 Global phytoplankton carbon biomass from SeaWiFS observations and CMIP5 models

The mission climatology of total phytoplankton carbon (C) biomass (Fig. 2a) indicates that algal biomass is lowest in the oligotrophic subtropical gyres, while higher biomass values occur in more eutrophic regions, such as the equatorial and eastern-boundary currents, other upwelling regions, as well as the high-latitude oceans. This general pattern corresponds to first order to the climatological Chl spatial patterns (Fig. A1) and is consistent with current oceanic ecosystem understanding (e.g. Longhurst, 2007). Comparison of the PSD-based approach to quantifying C biomass (Fig. 2a) with two existing methods (the B05 values, Fig. 2b, and the S08 POC retrievals divided by 3, Fig. 2c) reveal that the PSD-based approach results in a significantly wider range of spatial variability, as confirmed by the histograms in Fig. 3. The method of B05 resulted in the least spatial variability.

Among the three methods, the PSD-based biomass estimates are the lowest in the subtropical oligotrophic gyres (by about an order of magnitude) and highest (generally by less than an order of magnitude) almost everywhere north of $\sim 40^{\circ}$ N and along

OSD
12, 573–644, 2015

much of the west coasts of the Americas and Africa, in the north-western Arabian Sea and some portions of the Southern Ocean (most of the Atlantic sector, the northern and central parts of the Indian Ocean sector and in two zonal bands – one poleward and one equatorward – in the western Pacific sector). The three methods are in relatively good agreement in the Pacific equatorial upwelling region. A considerable difference also exists between the B05 and the S08-based values – the former vary the least spatially, mostly due to relatively high biomass estimates in the subtropical oligotrophic gyres.

While it is plausible that the PSD-based values in the oligotrophic gyres are underestimated and values in some eutrophic areas are overestimated, a global validation with concurrent field measurements of phytoplankton C biomass is not feasible at present since in-situ analytical measurements of phytoplankton carbon are difficult and made possible only recently by emerging techniques (Graff et al., 2012). The S08 method is developed with in-situ POC and reflectance data, and the constant conversion factor in B05 is picked empirically, so these algorithms are designed a priori to match in-situ measurements. The method presented here is derived mostly from theory (apart from the allometric relationships themselves) and is not subject to such constraints (Sect. 3.7.3). Importantly, even if the absolute carbon concentration values are inaccurate, the PSCs expressed as percent contribution to C biomass should still be reliable and subject to much less uncertainty (Sects. 3.3 and 3.7). This carbon-based absolute and fractional partitioning is provided here for the first time and the fractions can be used with other absolute carbon estimates.

The exaggeration of the global range of values of the PSD-based mean algal biomass field (Fig. 2a) as compared to the approach of B05 (Fig. 2b) is expected because the latter uses a single scaling constant to estimate carbon from backscattering, whereas the allometric method explicitly takes into account the variability in backscattering efficiency of particles with varying particle size. Qualitatively, the PSD method relaxes the assumption of a constant in B05 by taking into account the varying backscattering per unit cell volume (via the PSD estimate) and per unit carbon in the

OSD
12, 573–644, 2015

cells (via the allometric relationships). This is a major improvement, although it carries with it a series of assumptions that lead to added uncertainty, especially with the purposeful lack of empirical tuning. Quantitatively, according to Mie theory calculations, $b_{bp}(\lambda)$ normalized to volume of particles in the 0.5 to 50 µm range is three orders of magnitude higher when the PSD slope $\xi = 6$, as compared to when $\xi = 3$ (not shown). Thus, the same backscattering coefficient will be attributed to less particle total volume (and thus carbon) if the particles are relatively smaller in size (higher ξ), unless the allometric relationship dominates the result. Since PSD slopes are highest in the oligotrophic gyres (KSM09), the PSD-based approach is expected to exhibit smaller total volume of particles and thus smaller carbon concentrations as compared to the direct scaling with b_{bp} (443) in B05.

The CMIP5 models ensemble mean of phytoplankton C biomass (Fig. 2d) resembles the S08 POC-based estimate the most in spatial patterns and values, with somewhat lower values in the subtropical gyres, but not quite as low as the PSD-based method (Fig. 2a). Notably, the models yield higher values in the Pacific Equatorial Upwelling zone than any of the satellite data sets. Overall, the model data exhibit a similar range of spatial variability to the method of S08, higher than B05, and lower spatial variability than the PSD-based approach, which is not empirically tuned. CMIP5 model estimates of phytoplankton C biomass are independent of these satellite data sets because they are based on theoretical principles and calibrations with in-situ data (refs. in Table 2).

3.2 Global phytoplankton biomass stock

The three satellite methods (Fig. 3) and the CMIP5 models (Fig. 2d) can be further compared quantitatively by estimating total global phytoplankton biomass stock (Sect. 2.6). Since ocean color data are not vertically resolved, we assume that the vertical profile of phytoplankton biomass is uniform down to the mixed layer depth (MLD). Estimates from the SeaWiFS mission climatological fields are remarkably consistent (Fig. 4a), yielding between 0.2 and ~ 0.3 Gt C standing biomass stock (1 gigaton (Gt) = 10^{12} kg = 1 petagram (Pg)). The B05 method yields the highest estimate,

OSD
12, 573–644, 2015

whereas the models and the other two satellite methods are quite similar to each other. Biomass in open ocean areas (with the continental shelves excluded) accounts for most global biomass according to all estimates, but the models attribute very little biomass to the shelves as compared to the satellite methods, especially the PSD-based method. Since the satellite methods are based on different assumptions, our results suggest that future CMIP5 model improvements should focus on estimates of biomass in continental shelves. However, this model-data discrepancy could be due to the lower underlying spatial resolution of the models; in addition, the satellite estimates originate from the same sensor and satellite algorithms are often subject to larger uncertainties in coastal zones (especially the PSD-based approach). It is best to develop technology to measure C biomass in-situ (Graff et al., 2012) and inform both satellite algorithms and biogeochemical models.

The total phytoplankton biomass estimate based on mission composites can be considered globally representative since 99–100 % of the total ocean area (or area excluding the shelves) participates in the estimate (Fig. 4a). However, some bias remains because high latitudes are observable only in summer months (Fig. A2). As a result, monthly climatological estimates of biomass from the three satellite methods (Fig. 4b) represent less area (between ∼ 85 % and ∼ 95 % of the total) which varies with the seasons. The seasonal variation observed can thus be confounded by variation in the observed area. In order to alleviate the problem with varying observable area by SeaWiFS and estimate a more representative global seasonal cycle, areas not observed by SeaWiFS were gap-filled with the corresponding CMIP5 model ensemble data and the monthly global time series were recomputed (Fig. 4c). The main difference between Fig. 4b and c, is that the seasonal amplitudes of all four data sets are decreased. As a measure of seasonality, we consider the difference between the maximum and minimum values from Fig. 4b, as a percentage of the mean annual signal. From the satellite data sets, the B05 and S08 estimates exhibit stronger global seasonality (∼ 39 %) than our PSD-based approach (∼ 23 %). The PSD-based approach exhibits the highest percentage of biomass in the continental shelf areas of all data sets. The CMIP5

OSD
12, 573–644, 2015

models exhibit significantly stronger seasonality (~ 93 %) that the satellite data sets. Importantly, the models exhibit a single annual peak in the austral summer, whereas the satellite data sets indicate highest global biomass in the transitional months near the equinoxes. These differences in global seasonality of biomass stock between the satellite data and the models suggest that model representation may need improvement in areas that contribute substantially to the global biomass stock in certain parts of the year, such as the Southern Ocean and/or the North Atlantic. However, satellite data also have issues such as underestimation of Chl in the Southern Ocean (Dierssen and Smith, 2000; Garcia et al., 2005; Kahru and Mitchell, 2010), indicating that ocean color products in general may be suspect in this undersampled part of the ocean. The special bio-optical character of the Southern Ocean is evidenced elsewhere (Uitz et al., 2006), indicating that regionally tuned satellite algorithms may be required. The area is also hard to observe due to high latitudes and cloudiness. This stresses the need for high quality in-situ observations of this region that contributes significantly to the global biological pump (Marinov et al., 2008).

It is remarkable that the three satellite methods yield estimates that are very consistent with each other and with the CMIP5 model ensemble values, especially since the models are independent of the satellite data (refs. in Table 2). Furthermore, the novel PSD-based method is not empirically restricted or tuned a-priori and yields reasonable estimates. Admittedly, this globally spatially integrated result may be fortuitous due to cancellation of uncertainties with opposite signs in the oligotrophic vs. eutrophic areas, so it is not claimed that this result necessarily constitutes algorithm verification.

Globally integrated mixed-layer algal C biomass values have been previously obtained by integrating remotely sensed Chl vertically and converting it to C using an assumed Chl : C ratio. Such estimates range from 0.30 to 0.86 Gt C (Antoine et al., 1996; Behrenfeld and Falkowski, 1997b; Le Quéré et al., 2005). Antoine et al. (1996) provide the highest estimate. They integrated Chl profiles vertically from the surface to whichever was larger between MLD provided by Levitus (1982) and the depth where sunlight intensity diminishes to 0.1 % of its sea-surface value ($Z_{0.1\,\%}$). The MLD val-

OSD
12, 573–644, 2015

ues of Levitus (1982) are likely deeper than those of de Boyer Montégut et al. (2004) applied here, because the former are based on considerably larger threshold criteria (0.5 °C for temperature and 0.125 kg m^{-3} for density) than the latter (Sect. 2.6). Also, $Z_{0.1\,\%}$ can exceed MLD in warm oligotrophic waters, which cover a large proportion of the total ocean area. This was the case over ~ 60 % of the global ocean area in the study of Antoine et al. (1996); in these cases they employed non-uniform vertical profiles of Chl (Morel and Berthon, 1989). For these reasons, it is expected that the global ocean algal biomass estimate by Antoine et al. (1996) will be higher than the values we determined here. Similar reasoning holds for the respective estimates by Le Quéré et al. (2005) and Behrenfeld and Falkowski (1997b).

3.3 Size-partitioned biomass

A pivotal advantage of the novel PSD-based biomass algorithm, as compared to existing approaches, is the ability to partition carbon among any size classes. The absolute C biomass concentrations of picoplankton (Fig. 5a), nanoplankton (Fig. 5b) and microplankton (Fig. 5c) reveal a general global spatial pattern for all three size classes similar to the global total distribution (Fig. 2a), namely the lowest biomass values are encountered in the oligotrophic gyres, whereas higher latitudes, coastal and upwelling areas exhibit higher biomass. These are mission composites and do not reveal seasonality, and high latitude averages are overestimated due to many months of missing wintertime data (Fig. A2).

According to contemporary understanding of oceanic ecosystems (e.g., Uitz et al., 2010) we expect large cells (such as diatoms) to be opportunistic, responding via strong localized blooms to changes in nutrient inputs or grazing. This opportunistic response, which contrasts the smaller picoplankton adaptation to constant environmental conditions, explains the widely different spatial and temporal variability of these groups. Accordingly, we find that the range of spatial variability of carbon for picoplankton (< 3 orders of magnitude) is a lot smaller than the range of variability for nanoplankton (~ 4) and especially microplankton (~ 5 orders of magnitude) (Fig. 6). Negligible biomass is

OSD
12, 573–644, 2015

found in microplankton for most of the ocean area, except for eutrophic areas characterized by seasonal blooms and/or higher overall productivity such as the Equatorial Upwelling, whereas picoplankton are more globally ubiquitous.

The fractional contribution of each PSC to total C biomass reveals the climatological dominance of each group in the various oceanic regions (Fig. 7). The C-based fractional PSCs' spatial patterns are broadly consistent with contemporary understanding of phytoplankton biogeography. Thus, picoplankton emerge as the dominant size group in oligotrophic areas (Fig. 7a), because their large cellular surface-area-to-volume ratio enables them to acquire scarce nutrients very efficiently (Agawin et al., 2000; Falkowski and Oliver, 2007). By contrast, larger phytoplankton contribute relatively more biomass in the regions where nutrients are generally more abundant, because they can take up nutrients at a faster rate and store them inside vacuoles as a reserve for less favorable spells (e.g., Eppley and Peterson, 1979; Falkowski et al., 1998; Falkowski and Oliver, 2007). Together, nano- and microplankton achieve dominance (between 50 and 90 %) along the Antarctic coastline, in much of the zone between ~ 40 and $\sim 50^{\circ}$ S (in the South Atlantic, the south-western Indian Ocean, southeast of Australia and east of New Zealand), along the eastern boundaries of the Pacific and Atlantic Oceans, in the north-western Arabian Sea and almost everywhere north of $\sim 40^{\circ}$ N. The relative dominance of larger algal cells in high nutrient regions occurs even though C biomass of all PSCs, including picoplankton, increases in high-nutrient regions (Fig. 5), since rising nutrient concentrations cause a disproportionately greater growth in the biomass of larger phytoplankton cells (Raven, 1998).

The total biomass patterns in the Southern Ocean (Fig. 2a) are characterized by more or less continuous bands of high biomass (a) along the frontal structures around 40–45° S, a transitional region from the iron limited upwelling regime in the South to the nitrate limited downwelling subtropical gyres in the North and (b) in the marginal sea ice regions next to the Antarctic continent, where continental iron (Fe) inputs likely result in biomass and production spikes during the spring and summer. Both these large-biomass bands tend to be dominated by the larger opportunistic groups of nano

OSD
12, 573–644, 2015

and microplankton (Fig. 7b and c). In between these two bands of high production we find a relatively lower biomass band from roughly 50–60° S, where picoplankton thrive (Fig. 7a). The lower total biomass here is due to a combination of iron limitation and deep summertime mixed layers, resulting in strong light limitation during the growing season. Large areas in the Southern Hemisphere are characterized by lower total (Fig. 2a) and group-specific C biomass (Fig. 5a–c), as compared to the Northern Hemisphere. This interhemispheric disproportionality is dominated by high-latitude summer values (not shown) and is in agreement with findings that the Southern Ocean sustains relatively low phytoplankton biomass, in spite of high ambient macronutrient concentrations (e.g., Dugdale and Wilkerson, 1991).

We emphasize that even though other approaches for quantifying total phytoplankton carbon (C) biomass from space have been published (B05; S08 (as adapted for use in our study), Sathyendranath et al., 2009), our methodology is unique in its ability to partition biomass defined in terms of carbon in any desired size classes. Given the first order correspondence between PSCs and PFTs (however, note that they are not the same – e.g. Brewin et al., 2011; Hirata et al., 2012; Nair et al., 2008), various existing algorithms that retrieve PFTs (IOCCG, 2014) can be qualitatively compared to the PSD algorithm. Among those algorithms, the PSD-based method is again unique in defining the PFTs as fractions of carbon biomass, the most biogeochemically relevant quantity. Notably, Roy et al. (2013) also retrieve the PSD power-law slope (like KSM09), but from absorption, and define their PFTs as Chl fractions. Direct quantitative comparison among the various PFT/PSC algorithms is not always trivial because PFTs/PSCs are defined differently and, are based on different variables and different parameterization data sets and assumptions. Kostadinov et al. (2010) briefly compare the PSD-based volume fractions from the KSM09 algorithm with the PFT retrievals of Uitz et al. (2006) and Alvain et al. (2008). Brewin et al. (2011) describe the first round of PFT algorithm intercomparisons. The International PFT Intercomparison Project (Hirata et al., 2012, 2015) is currently in progress and is tasked with an extensive quantitative algorithm comparison, which is outside the scope of this work.

OSD
12, 573–644, 2015

3.4 In-situ POC-PSD closure

While a direct validation of the PSD-based phytoplankton carbon retrieval is not feasible on a global scale due to the lack of in-situ data and established measurement protocols (Graff et al., 2012), it is instructive to test the closure between in-situ determinations of POC and the PSD. Such analysis would serve as a form of validation, i.e. proof of concept, for the satellite algorithms and it also has the advantage of not being subject to the usual issue of remote sensing validation, importantly the mismatch of the scales of measurement and the uncertainty in the radiometric quantities and the bio-optical algorithm assumptions and uncertainties. Unfortunately, even concurrent in situ POC and PSD measurements are rare, especially in the open ocean. Here we test closure between two different ways to compute phytoplankton carbon from AMT cruise 2, 3, and 4 measurements: (1) a chemical POC determination, divided by 1/3, and (2) Coulter Counter PSD measurements, which are used to calculate allometric carbon concentrations in the same way that satellite PSD's are (Sect. 2.1). Two different sets of integration limits (Eq. 4) for the power-law PSD are tested: 0.5 to 50 µm (Fig. 8a) and 0.7 to 200 µm (Fig. 8b). The first set of limits was chosen to match the operational satellite carbon algorithm. The second set of limits was chosen to match the operational in-situ POC measurement: the nominal pore size of GF/F filters used in field measurements of POC and optical properties (e.g. S08; Kostadinov et al., 2012) is 0.7 µm, and the water was also pre-filtered with a pore size of 200 µm, so only the 0.7 to 200 µm fraction is measured as POC.

The R^2 of the regression (in log10-space) for the first set of limits (Fig. 8a) is better, but the slope, bias, and RMS are better for the latter limits (Fig. 8b). In both cases the regressions are highly significant ($p < 0.01$), indicating that the volume and carbon content of particles measured in natural seawater via the total PSD can reasonably predict the chemical determination of carbon content. The PSD method is sensitive to the chosen limits of integration, and the satellite operational limits underestimate the POC-based values. This underestimation is reduced, but not fully eliminated when the

OSD
12, 573–644, 2015

0.7 to 200 µm limits are used; the data are visually much closer to the one to one line (cf. Fig. 8a and b). This indicates that correspondence is better when the limits match the nominal pore size of the filter used. This is encouraging, since it indicates that with entirely in-situ data, reasonable closure, i.e. internal consistency, exists between two very different methods of in-situ assessment of living carbon. A relatively good in-situ POC-PSD agreement was also confirmed by Kostadinov et al. (2012) for most data points collected a semi-arid coastal site – the Santa Barbara Channel (SBC) off of California. Their result lends further support to the formulation of the algorithm presented here – in spite of the SBC being an optically complex coastal site where terrigenous materials can influence optical properties (Toole et al., 2001; Otero and Siegel, 2004; Kostadinov et al., 2007), a good POC-PSD closure exists.

Clearly, the estimation of phytoplankton carbon from the total PSD or from POC in-situ is subject to some of the same uncertainties and limitations as the satellite algorithm (allometric equations, applying living cell relationships to all particles, factor of 1/3 variability, power-law assumption, limits of the Coulter Counter measurement, etc.). This introduces errors, so a more perfect correspondence is not realistic. Section 3.7 discusses such assumptions and uncertainties in detail.

3.5 Carbon-based vs. volume-based PSCs

The carbon-based PSCs constitute a recast of the volume fraction PSCs of Kostadinov et al. (2010). As such, both are PSD-based and are only functions of the PSD slope ξ (the N_o parameter cancels when taking the ratio of Eq. 5 for different size classes), for a given set of allometric coefficients and size limits of integration. This recast to carbon via the allometric relationships leads to a modification of the functions but a preservation of their general shape and tendencies as a function of ξ (Fig. 9). The values of the allometric coefficients are a reflection of the fact that smaller phytoplankton cells are more carbon dense than larger cells (MDL2000; Moal et al., 1987; Verity et al., 1992). According to the relationships in MDL2000, the tiniest phytoplankton (ESD = 0.5 µm) contain close to 5.5 times more carbon per unit cell volume than the largest phyto-

OSD
12, 573–644, 2015

plankton cell considered in this study (ESD = 50 µm) (Fig. 1). This results in higher C-based picoplankton fractions when they are based on C as compared to volume-based ones, for all PSD slopes, and the opposite is true of microplankton (Fig. 9). The sign of this difference depends on the PSD slope for nanoplankton, but for most of the ocean ($\xi > \sim 3.5$) C-based nanoplankton fractions are lower than volume-based values, with the exception of some limited areas with very low PSD values, such as the northern North Atlantic, the confluence zone of the Brazil and Falkland/Malvinas Currents and the thin coastal bands of the Weddell and Ross Seas (not shown).

3.6 Relationship between phytoplankton carbon biomass and chlorophyll concentration

Qualitative assessment of spatial distributions of Chl (Fig. A1) suggest positive correlations with the spatial patterns of C biomass (Fig. 2a), as well as nano- and microplankton fractions (Fig. 7b and c), whereas there is a negative correlation with picoplankton fraction (Fig. 7a). The bivariate histogram of Chl vs. total C biomass (Fig. 10a) confirms this strong correlation. However, for a given Chl value, total biomass can vary considerably (over an order of magnitude for some less frequent values). For example, for the common Chl value of $\sim 0.25\,mg\,m^{-3}$, biomass frequently varies between 10 and $30\,mg\,m^{-3}$, a three-fold difference, and for some less frequent values it can be as low as $\sim 1\,mg\,m^{-3}$ or as high as $\sim 100\,mg\,m^{-3}$. Although some of this spread may stem from underlying uncertainties in C biomass (Sect. 3.7) and Chl (Gregg et al., 2009; Sathyendranath, 2000), much of it is likely attributable to ecological variability that is captured by taking into account the particle-size-distribution (PSD), particularly because the areas associated with the highest expected uncertainties in the PSD method (i.e. continental shelves (KSM09)) were excluded from this analysis. This confirms that the PSD-based biomass retrieval method brings valuable new information, and is not merely a deterministic function of Chl alone.

Clearly, Fig. 10a confirms that to first order, Chl can serve as an indicator of photosynthetic biomass (e.g., Behrenfeld and Falkowski, 1997a). However, there are at least

OSD
12, 573–644, 2015

two separate processes that can drive this relationship, namely physiological changes in Chl without accompanying biomass changes (e.g. photoacclimation), and/or actual biomass growth with increasing Chl. That is, Chl can also fluctuate independently of C biomass, in response to variability in the ambient levels of light, nutrients and temperature (e.g. Geider et al., 1998). The extent of such physiological fluctuations depends not only on the degree of environmental variations, but can also be influenced by the size and taxonomic association of phytoplankton cells (Geider, 1987; Landry et al., 2000; Pérez et al., 2006). It is therefore also expected that a broad range of biomass values can correspond to a single Chl estimate from our method, and vice versa (Fig. 10a).

The histogram of Fig. 10a exhibits a pronounced sigmoidal shape in logarithmic space. The part of the curve corresponding to low and medium Chl values is consistent with the conjecture that physiology, rather than biomass growth and loss, is the main driver of Chl variability in oligotrophic, lower latitude region, whereas Chl changes in eutriphic, higher latitude areas are accompanied by biomass changes (B05; Behrenfeld et al., 2006; Siegel et al., 2013). B05 observe that for low Chl, "background" low values of $b_{bp}(440)$ do not covary strongly with Chl; then for higher Chl values there is a positive linear correlation which tends to level off a bit for high Chl values (see their Fig. 1). Thus our observed Chl to C biomass global relationship is broadly consistent with the B05 Chl to backscattering relationship, confirming their (and our) choice to use backscattering as a first order proxy of biomass. The PSD-based method here builds on this concept further by relaxing the assumed constant relationship of backscattering to particle volume/mass by taking into account the underlying PSD that produced the backscattering. This constitutes the key contribution of the novel PSD-based algorithm.

Bivariate histograms between Chl and the fractional PSC's (Fig. 10b–d) indicate that the picoplankton fraction (Fig. 10b) decreases with increasing Chl, whereas nanoplankton (Fig. 10c) and microplankton (Fig. 10d) fractions increase. The pico- and nanoplankton relationships also exhibit the sigmoidal shape, and the picoplankton is basically roughly equivalent to the sigmoid of Fig. 10a with an inverted *y* axis, because there is a strong negative correlation between absolute total biomass and the fraction

OSD
12, 573–644, 2015

due to picoplankton. All of the above observations are consistent with the premise that oligotrophic areas (low Chl) are dominated by smaller cells and eutrophic areas (high Chl) – by larger cells (e.g. Chisholm, 1992; Falkowski et al., 1998; Kostadinov et al., 2010). The considerable noise in these relationships is most likely due to the natural ecosystem variability that occurs for a given Chl value – i.e. ecosystem structure and species composition can vary globally even for a given Chl value, illustrating that (1) the PSD-based algorithm adds new, independent and valuable information to ecosystem characterization and (2) PFT algorithms based on Chl abundance (IOCCG, 2014, e.g. Brewin et al., 2010; Hirata et al., 2011; Uitz et al., 2006) may miss this variability. The variability in Fig. 10b–d for a given Chl value is less likely to be due to uncertainties, because the uncertainties in the fractions are considerably smaller than for the absolute carbon values, especially for the climatological imagery (Sect. 3.7.1).

The relationships between C-based PSCs and Chl are broadly consistent with the observations of Hirata et al. (2011). They derive the same relationships using global in-situ HPLC measurements, and their PSC are based on fractional contributions to Chl, not C biomass. For picoplankton, they also observe a sigmoid curve, but it is inflected the opposite way from our Fig. 10b. This could be due to the fact that physiological adaptations may lead to changes in pigment composition without changes in size structure or carbon biomass. A fruitful approach for further investigation would be to focus on blending these two approaches to derive more information about oceanic ecosystems. Both approaches agree remarkably well on the general shape of nanoplankton contribution as a function of eutrophic state (cf. our Figs. 9 and 10c with their Fig. 2b), indicating maximum nanoplankton fraction at transitional, intermediate eutrophic states, with nanoplankton never exceeding about 50 %. This is encouraging because this limit of the PSD-based model is a result of the mathematical formulation, whereas the Hirata et al. (2011) result is based on empirical diagnostic pigment observations. However, the shape of this curve is not well observed for high Chl values on the bivariate histogram (Fig. 10c) and Hirata et al. (2011) observe a higher maximum than the PSD method. Finally, for microplankton the curve shapes agree well, but Hirata et al. (2011) fractions

OSD
12, 573–644, 2015

reach values up to 80 % for high Chl, whereas our PSD-based algorithm rarely exceeds 50 % (cf our Figs. 9 and 10d with their Fig. 2c).

3.7 Uncertainty propagation and budget

There are multiple steps involved in the retrieval of the carbon-based biomass products presented here. Namely, starting with top of the atmosphere radiance observed by the sensor, normalized remote-sensing reflectance are obtained after atmospheric correction, then spectral backscattering coefficients are retrieved via the LAS2006 algorithm, after which the LUTs of the KSM09 algorithm are applied to obtain the power-law PSD parameters, which in turn are used to estimate particle volume, which is converted to phytoplankton carbon using the MDL2000 allometric relationships. Each of the above steps is associated with a set of assumptions and uncertainties, some of which are not quantifiable at present. The uncertainties at each step combine with those of the previous steps and propagate to the final products. Below, we (1) make a quantitative assessment of propagated quantifiable uncertainties of the retrieved carbon-based products, (2) assess the sensitivity of the products to the PSD parameters, and (3) offer a general discussion of algorithms assumptions and other unquantified uncertainties.

3.7.1 Propagated quantifiable uncertainties

KSM09 provide a Monte Carlo assessment of endogenous uncertainties of the PSD algorithm products, i.e. uncertainties that are due to natural variability of the input parameters to Mie theory – the complex index of refraction and the maximum diameter of the particles considered. The allometric parameters of MDL2000 are another source of uncertainty which is quantified as the statistics of the regressions used to derive them. These partial uncertainties of the input parameters to the carbon algorithm were propagated to the final algorithm products discussed here (Sect. 2.5, Eq. 6). Note that covariances among the input parameters are ignored in Eq. (6), which can lead to under- or overestimation depending on the signs of the covariance and the deriva-

OSD
12, 573–644, 2015

tives. Importantly, the process of averaging when producing composite imagery further reduces random errors (Eq. 7), but not consistent bias (e.g. Milutinović and Bertino, 2011). Therefore, uncertainties in a single image produced from the input parameters are qualitatively different from uncertainties in a composite image produced by averaging multiple carbon product images with individually propagated errors. In this work we produce PSD-based products from monthly SeaWiFS imagery and propagate errors to each monthly image. The errors in any composite imagery are then calculated from the errors of the individual images participating in the averaging. Absolute uncertainties are discussed here in terms of one standard deviation, in the same units as the variable.

Averaging was not weighted by the inverse of the variance (σ^{-2}) in composite imagery as it was done by Maritorena et al. (2010) (their Eq. 2) so as to not bias the data to lower values. This is because this weighting is only appropriate when the measurements from the same underlying random value distribution are made (i.e. on a spatio-temporal scale on which the ocean is not expected to change intrinsically, S. Maritorena, personal communication, 2015), and further because our error structure is such that error values are proportional to the value of the retrieved parameter (the latter is especially true for the absolute carbon retrievals, and much less so for the fractional PSCs).

Uncertainty in the total phytoplankton C biomass mission composite (Fig. 11a) is higher in eutrophic regions than in oligotrophic ones and does not exceed $\sim 1\,\mathrm{mg\,C\,m^{-3}}$ over most of the ocean, except in high latitude areas and some eutrophic areas. At high latitudes the individual monthly errors are larger and there are less monthly data available for averaging (Fig. A2). Examination of relative uncertainty for the global composite image indicates that it rarely exceeds 20 %, except for the very high latitudes (prominently south of 60° S and in the Arctic Ocean), and in the oligotrophic gyres, where some pixels exceed ~ 50 % relative uncertainty (not shown). The gyres are characterized by noisy uncertainty patterns (large variability on the pixel scale, not shown).

OSD
12, 573–644, 2015

The relative uncertainty of a typical individual monthly image is between 85 and 115 % globally, illustrating the significant uncertainty reduction of the composite image (Eq. 7).

The uncertainty of the mission composite fractional picoplankton contribution to carbon biomass is very low (Fig. 11b), less than ∼ 1 % over most of the ocean, and not exceeding ∼ 7 % anywhere. The uncertainties for the other PSC's are similar (somewhat higher for microplankton, but only at the very high latitudes, not shown). Individual imagery uncertainty for the fractional picoplankton vary between ∼ 3 % to ∼ 8 % (1–7 % for nanoplankton fractions, and ∼ 0–2 % for microplankton, higher in eutrophic areas), illustrating that even for individual images fractional PSC uncertainties are quite low. This result is expected because the N_o parameter, which is a large source of error (see below), cancels in computation of fractional PSC's (Eq. 5). This result is similar to the findings of KSM09 for the volume-based fractional PSC's. The carbon-based PSC's are likely to be a reliable product even if absolute carbon concentrations are not accurate. For this reason the carbon-based fractional PSC's are considered the more reliable and important product presented here. In fact, these PSC's can readily be used to partition other, independent estimates of phytoplankton carbon, such as those from the algorithms of B05 and S08, or even climate model data. Further discussion of this can be found in Sect. 3.7.3.

Analytical error propagation (Eq. 7) permits tracing the relative contribution of the various input variables to the uncertainty of the dependent variable. Uncertainties are additive in quadrature, i.e. total variance is the sum of the variance due to its various sources (Eq. 7). Thus, contribution to total uncertainty is easily expressed as percent contribution to the total variance. Fractional contributions to uncertainty were analyzed for an example month, namely May of 2004. The sources of error for total C quantified here are errors in the PSD parameters, ξ and N_o, and errors in the allometric coefficients. Almost the entire variance (> 95 % nearly everywhere) in total carbon is driven by uncertainties in N_o (Fig. 12a). The remainder is mostly due to the allometric coefficients in oligotrophic areas (Fig. 12b), and only in some limited eutrophic areas the

OSD
12, 573–644, 2015

PSD slope ξ has a non-negligible contribution to total C variance (the three contributions sum to 100 % of the error, so the map for ξ is not shown).

The fractional PSCs total uncertainty depends on uncertainties in the PSD slope and the allometric coefficients. For the oligotrophic gyres and some transitional areas around them, most of the uncertainty in picoplankton fraction is due to the allometric coefficients (Fig. 12c), whereas for the higher latitudes and productive areas ~ 80 % of the variance is due to the PSD slope. For the nanoplankton fraction, almost everywhere the uncertainty is mostly due to the allometric coefficients, since the derivative of nanoplankton fraction with respect to ξ is small over most of the ocean (Fig. 9). For microplankton in oligotrophic areas, the error is due almost exclusively to the allometric coefficients, but in eutrophic areas it is usually about equally due to the allometric coefficients and the PSD slope.

3.7.2 Sensitivity to PSD parameters and the limits of integration

We next investigate the sensitivity of the carbon-based products to the input parameters, i.e. the PSD parameters and the limits of integration of Eq. (4). Only the upper limit, D_{max}, is analyzed because there are firm biological reasons to set the lower limit at D_{min} = 0.5 µm (Sect. 2.1.2), while the upper limit is ambiguous (e.g. Sieburth et al., 1978; Brewin et al., 2010; Uitz et al., 2006; Aiken et al., 2008). Note, however, that Hirata et al. (2011) and Roy et al. (2013) use different picoplankton limits. This sensitivity analysis is important because total uncertainties are a function not only of the uncertainties of the inputs, but also of the derivatives of the outputs with respect to the inputs (Eq. 6).

The effect of varying D_{max} from the operational value of 50 to 200 µm is largest for low PSD slopes (Fig. 13a) and does not exceed ~ 25 % for fractional C-based nanoplankton, somewhat less for microplankton, and much less for picoplankton. The effect diminished quickly for larger PSD slopes and is quite small for $\xi > 4$ (covering most of the ocean, see histogram in Fig. 13a). Using the operational limit globally may cause an underestimation of microplankton contributions and instead may attribute this car-

OSD
12, 573–644, 2015

bon mostly to nanoplankton, in the eutrophic productive areas of the ocean, during episodes when cells substantially larger than ~ 50 µm ESD are present in the bloom. The present algorithm is a proof-of-concept approach that is optimized for global applications, and there are reasons to believe the operational D_{max} choice is the best (Sect. 2.1.2).

Total phytoplankton carbon concentration is a relatively weak function of the PSD slope (Fig. 13b), especially around $\xi = 4$, where the derivative changes sign. There is less than an order of magnitude variability in carbon over the entire range of PSD slope values. In contrast, total carbon is a very strong (linear in log space) function of the N_o parameter (Fig. 13c), leading to ~ 4 order of magnitude variability with the realistic values for N_o. This is a very critical finding, illustrating than total carbon concentrations are driven mostly by N_o; in addition, the uncertainties in N_o are relatively higher and spatially uniform themselves (KSM09), accounting for most of the uncertainty in total carbon (Fig. 12a). To first order, efforts to improve carbon retrievals thus need to focus on N_o rather than other sources of error. N_o has a similar effect (linear in log space) on the carbon concentration in the different PSCs (Fig. 13c). The effect of varying D_{max} is also shown, indicating that microplankton carbon is the only value affected more significantly, but only within much less than an order of magnitude. In contrast, carbon in the different PSCs is a different function of ξ for each PSC (Fig. 13b), illustrating large variability for microplankton and smaller variability for pico- and nanoplankton. As expected, increasing the PSD slope allocates more carbon to the smaller PSCs (at a fixed N_o). D_{max} variability only affects microplankton and total carbon concentrations at low PSD slopes (Fig. 13b), and this variability is generally smaller than the quantifiable uncertainties (cf. Figs. 11a and 13b), unlike the effect of D_{max} on fractional PSCs, which can be larger than the quantifiable uncertainties for low PSD values (cf. Fig. 11b and 13a).

OSD
12, 573–644, 2015

3.7.3 Model assumptions and additional sources of uncertainty

The propagated quantified uncertainties (Sect. 3.7.1) are only partial estimates of the total uncertainty budget, as there are additional sources of uncertainties that can affect the operational carbon products. Here we briefly discuss the model assumptions and some of these additional not necessarily quantifiable uncertainty sources.

The radiometric ocean color products (i.e. SeaWiFS $R_{rs}(\lambda)$ in this case), which are the initial input for the biomass algorithm, are associated with their own uncertainties, as is the output of the LAS2006 algorithm. These uncertainties are not easy to quantify on a per-pixel basis and are not provided directly by the algorithm developers. Loisel et al. (2006) provide a detailed analysis of error sources for the spectral slope of backscattering. These uncertainties are not included in the error budget presented here. However, efforts are currently underway to provide a reasonable quantification of the effect of those uncertainties on the estimated spectral backscattering and its slope, and thus on the PSD and all downstream products. Note specifically that reflectance uncertainties would propagate in complex, non-linear ways to the spectral slope of backscattering, as it is a secondary parameter, sensitive to errors across all used wavelengths.

The PSD parameters are retrieved from the products of the LAS2006 algorithm via LUTs, which incorporate certain assumptions and uncertainties as well. A detailed analysis of exogenous sources of uncertainties in the PSD parameters is provided in KSM09. Here, a brief summary of the important points is provided. The KSM09 algorithm assumes a power-law PSD as does the calculation of particle volume itself (Eq. 4). While there are some indications that deviations from the power-law can be significant, especially in coastal waters (Reynolds et al., 2010), it remains a good first-order approximation especially in global applications (KSM09 and refs. therein). Furthermore, the applicability of the power-law is assumed to hold over the entire diameter range of optically significant particles, including submicron particles, for which measurements are very scarce. Mie scattering theory (Mie, 1908) assumes spherical

OSD
12, 573–644, 2015

and homogeneous particles, even though it is clear that these assumptions do not often hold for living phytoplankton cells. Violations of these Mie theory assumptions are likely to be more severe in coastal and eutrophic areas where larger cells increase in importance (KSM09). To date, the backscattering budget is not satisfactorily closed (e.g. Stramski et al., 2004), i.e. there is considerable uncertainty in the sources of backscattering and their relative importance. The difficulty lies in the complexity and variability of the suspended particle assemblages in natural waters, and the limited theoretical abilities to model scattering (Quirantes and Bernard, 2004; Clavano et al., 2007). Recent studies indicate that large phytoplankton may be responsible for more backscattering than Mie theory predicts (Dall'Olmo et al., 2009), and that significant fraction of backscattering variance is explained by nanoeukaryotes (Martinez-Vicente et al., 2013).

The retrieval of phytoplankton C biomass from PSD relies upon several further key assumptions. For absolute C retrievals, we assume that all particles belong to the POC pool (i.e. that they are biogenic in origin) and that that the proportion of phytoplankton in POC is constant (i.e. equal to 1/3 of POC by mass), as well as that the allometric coefficients apply to the heterotrophic and non-living (detrital) pools as well. Some of these assumptions are inherited from the interpretation of the PSD-determined volume as biogenic (Kostadinov et al., 2010). For the calculation of the fractional PSCs, the factor of 1/3 cancels, which is equivalent to assuming a less stringent variable factor, as long as it is constant for a single observation (pixel) across all the size classes. A contribution from non-biogenic particles and non-autotrophic POC would also cancel as long as it is in constant proportion (as converted to C) across the size classes, but is nonetheless less stringent than the ones for absolute C. This assumption is akin to the one made for volume-based PSCs by Kostadinov et al. (2010); both assumptions are more stringent than the classical Case I bio-optical assumption (Smith and Baker, 1978; Siegel et al., 2005). The assumption of biogenic nature of the particle assemblage is most likely to be violated in shallow coastal waters where processes such as river discharge, wind-driven dust deposition and tidal mixing can introduce large and

OSD
12, 573–644, 2015

variable amounts of inorganic particles into the water column (e.g. Otero and Siegel, 2004). As many of the other uncertainties are likely to be largest in the coastal ocean, the continental shelves were excluded from some of our analyses.

Some of the above assumptions are necessary artifacts of the model formulation and clearly have no theoretical basis, such as the application of allometric conversion to non-phytoplankton particles. Others can be improved upon by more detailed knowledge of the ecosystems being studied, e.g. the 1/3 factor and the shape of the PSD. Addressing these assumptions will require more observations and theoretical developments. The algorithm presented here is a first order, proof-of-concept approach meant for global applications. Additional knowledge of the ecosystems being studied can be used to improve the estimates, for example if diatoms are known to be dominating a bloom based on an additional source of information, the allometric relationships specific to diatoms can be applied preferentially instead. Taking a more integrated approach to PFT assessment has been studied (Raitsos et al., 2008), and future efforts should explore the possibility to leverage knowledge specific to biomes that are allowed to vary in time and space (Fay and McKinley, 2014) to tune the algorithm for them, including the underlying PSD LUTs (see below). Furthermore, dynamic assessment of the POC : living C ratio should become more operationally feasible as more concurrent data become available from the field (Graff et al., 2012).

As emphasized already, the expression of the PSCs in relative terms as fractions of C biomass has the distinct advantage of being only a function of the PSD slope ξ (for a given set of the allometric coefficients and limits of integration), since N_o cancels out. Since N_o is subject to larger uncertainties (KSM09) and it drives total carbon values to first order (Fig. 13c), it is expected that the fractional PSCs are a more reliable and robust product. In contrast, caution should be exercised when interpreting and using absolute carbon values. The main source of uncertainty in N_o is the real part of the index of refraction of the particles, n_p, which is allowed to vary over a wide range in the KSM09 algorithm development. According to Mie theory, fewer particles with a higher real refractive index will cause the same amount of backscattering as would more par-

OSD
12, 573–644, 2015

ticles of smaller refractive index and otherwise the same characteristics (e.g. Wozniak and Stramski, 2004). This is confirmed in observational data sets (Neukermans et al., 2012). Therefore, the wide range of n_p used in the KSM09 LUT construction (1.025 to 1.2) results in large uncertainty in N_o retrievals, which is a measure of particle number concentration. A single LUT is applied globally in the KSM09 algorithm. In the open ocean, for example the oligotrophic gyres, mineral particle influences are expected to be minimal and thus n_p would be closer to 1.05, characteristics of organic particles, rather than closer to 1.2, which is characteristic of mineral particles (e.g. Wozniak and Stramski, 2004). Therefore, by assuming larger overall values for n_p the LUT in KSM09 is likely to underestimate N_o over the open ocean (by attributing the backscattering to fewer particles of higher n_p than reality), and conversely, to possibly overestimate it in coastal areas where mineral particle influence could be more substantial. This may explain the spatial range exaggeration seen in the PSD algorithm's retrieval, as compared to the other satellite approaches or the models (Fig. 2). The KSM09 algorithm was designed for global operational applications (as is the carbon algorithm presented here), but it is expected that regionalizing the LUT based on a priori knowledge of the specific particle assemblages will improve performance. Importantly, this is the primary direction for improvement of our retrievals of absolute carbon concentrations, as N_o contributes to most of the uncertainty (Fig. 11a). Future research should also explore the feasibility of applying the relationship of the real index of refraction to intracellular carbon concentration (Stramski, 1999) in conceptually different scattering modelling that uses this relationship to model n_p, rather than treating it as a source of random error as in KSM09. The feasibility of such an approach may improve with the advent of global space-borne hyperspectral ocean color sensors such as PACE.

In contrast to the absolute concentrations, fractional PSC uncertainty is driven predominantly by uncertainties in the allometric coefficients over much of the ocean, and sometimes the PSD slope. Thus, improvements in the fractional PSCs should focus mostly on the allometric coefficients, which come with their own set of assumptions and sources of error, only some of which are quantified as the regression coefficients'

OSD
12, 573–644, 2015

confidence intervals in MDL2000, i.e. the dispersion of the data around the statistical fit. Sources of such errors could be, for example, combining the data coming from fixed and living cells, autotrophs and heterotrophs, and different morphology (thecate vs. athecate dinoflagellates). Other factors that contributed to the variance of the MDL2000 data set were (details in MDL2000): errors in cell dimension and C content measurements, deviations of cell shapes from the geometric approximations used to compute volume and considerable inter- and intra-specific variability in $C_{cell} : V_{cell}$ ratios. This variability necessitates the use of different allometric relationship for diatoms and other non-diatom large cells (Fig. 1). This choice is based on the recommendation of MDL2000 that the biomass of mixed plankton be determined by using one equation for diatoms and another for the remainder of unicellular plankton, treating cells above and below $V_{cell} = 3000\,\mu m^3$ differently. The assumption of equal contributions of diatoms and non-diatoms to the total carbon pool for cells larger than this threshold volume is not expected to hold globally everywhere, and should be relaxed in the future by combining with other PFT methods capable of detecting diatoms (e.g. Hirata et al., 2011) and/or integrated ecosystem approaches based on regional knowledge (Raitsos et al., 2008; Fay and McKinley, 2014).

Additional uncertainties exist that are external to the MDL2000 data set and therefore not included in their variance estimates. For instance, it is not clear how representative these data are of natural phytoplankton assemblages. The MDL2000 allometric relationships are based mostly on eukaryotes, with only two data points contributed by cyanophytes (prokaryotic). The bacteria are thus underrepresented in the derivation of the allometric relationships, and they are likely to be important, especially in oligotrophic waters. In addition, the diameter range over which the MDL2000 relationships were derived was ~ 1.4–$200\,\mu m$, indicating that we are extrapolating these relationships a bit on the lower end, for submicron particles. Clearly, more laboratory work is required to determine reliably the carbon content of small cells, especially since Stramski (1999) observe large uncertainties comparing allometric estimates to their carbon estimates (Stramski et al., 1995) for *Synechococcus*.

OSD
12, 573–644, 2015

Growth conditions and growth phase could also significantly affect $C_{cell}:V_{cell}$ ratios (Davidson et al., 2002). For example, the dinoflagellate cells that MDL2000 used to derive $C_{cell}:V_{cell}$ relationships were grown in nutrient-replete cultures at a fixed temperature and light-dark cycle, and were harvested during exponential growth phase. However, natural habitats often do not provide ideal conditions that can support continued exponential growth. Mesocosm experiments conducted on a natural plankton community suggest that both nutrient limitation and the proportions of macronutrients may have considerable impacts on cellular C concentrations (Davidson et al., 2002). Moal et al. (1987) observed a drop in cellular C concentration by between ∼ 10 and ∼ 60 % after undergoing a shift from exponential to stationary growth. Stramski et al. (1995) observed diel variations in cellular carbon content and intracellular carbon concentration for *Synechococcus* grown under natural light-dark cycles.

4 Summary and conclusions

We presented a novel method to retrieve phytoplankton carbon biomass from ocean color satellite data, based on combining volume determinations using backscattering-based PSD retrievals of Kostadinov et al. (2009) with carbon-to-volume allometric relationships compiled by Menden-Deuer and Lessard (2000). We use monthly SeaWiFS data to estimate total and size-partitioned absolute and fractional C biomass in three PSCs – pico-, nano- and microplankton. These PSCs can be treated as PFTs to first order. The climatological spatial patterns of the C-based PSCs broadly agree with current knowledge of phytoplankton biogeography and ecology. While the many steps and assumptions involved in arriving at the final algorithm products create considerable uncertainties, it is encouraging that without any a priori empirical restrictions, our estimates of global carbon biomass stock are consistent with other satellite algorithms and the CMIP5 Earth System models ensemble mean.

While there are other remote sensing methods capable of producing algal biomass or PFT estimates, our methodology is unique and novel in the following key ways: (1)

OSD
12, 573–644, 2015

ability to partition algal community biomass into any number of desired size classes in terms of absolute or fractional carbon concentration, which is the most relevant variable of interest in terms of biogeochemistry and is the unit of quantification of phytoplankton in Earth system models, (2) building on the concept of constant backscattering to carbon relationship of Behrenfeld et al. (2005) by explicitly taking into account the underlying PSD that produced the backscattering and thus relaxing the assumed constant relationship. We demonstrate that satisfactory in-situ closure is observed between PSD and POC measurements, which supports the PSD/allometric approach we take here.

Detailed uncertainty analysis indicates that total carbon concentration retrievals are sensitive to assumptions about the underlying bulk particle index of refraction, which may lead to exaggeration of the spatial range of concentration, calling for caution when interpreting absolute concentrations. Fractional PSCs, which are more reliable than the absolute carbon values, are subject to much smaller uncertainties due mostly to uncertainties in the allometric coefficients. The bio-optical algorithm presented here is a first-order, global, proof-of-concept approach that can be improved in multiple ways by addressing its assumptions and sources of uncertainty and incorporating new advancements in laboratory and satellite techniques (e.g. in-situ phytoplankton carbon measurements and space borne hyperspectral ocean color sensors).

5 Data availability and archival

Monthly and mission SeaWiSF composites of the PSD-based carbon biomass products will be archived in the PANGAEA data repository and will be publically available at [link or citation/instructions to be provided when available]. The following variables are provided: total carbon biomass (mg C m^{-3}), carbon biomass in the three PSCs (mg C m^{-3}), and the fractional contribution of the three PSCs to the total biomass (unitless). The PSCs are picoplankton (0.5–2 µm ESD), nanoplankton (2–20 µm) and microplankton (20–50 µm). The uncertainties associated with each variable are provided as one standard deviation in the same units as the variable. Note that these are partial uncertainty

OSD
12, 573–644, 2015

estimates of the corresponding composite (average) image, calculated from the partial uncertainties of the individual monthly imagery that participated in the average.

Acknowledgements. This work is supported by NASA Ocean Biology and Biogeochemistry Grant #NNX13AC92G to I. Marinov and T. S. Kostadinov. Grants NNG06GE77G, NNX08AG82G and NNX08AF99A also funded T. S. Kostadinov for parts of this work. T. S. Kostadinov is indebted to David Siegel and Stéphane Maritorena for multiple discussions and input that inspired and improved this work. We thank Brian Hahn, Dave Menzies and Danica Fine for help with data processing, and Peter Perkins for his bivariate histogram script. We acknowledge the NASA Ocean Biology Processing Group (OBPG) for maintaining and providing the SeaWiFS data set. We acknowledge the British Oceanographic Data Centre (BODC) for providing the AMT Cruise PSD and POC data. We acknowledge the World Climate Research Programme's Working Group on Coupled Modelling, which is responsible for CMIP, and we thank the climate modelling groups (listed in Table 2 of this paper) for producing and making available their model output. For CMIP the US Department of Energy's Program for Climate Model Diagnosis and Intercomparison provides coordinating support and led development of software infrastructure in partnership with the Global Organization for Earth System Science Portals. Additional ancillary data providers are indicated in the text.

References

Agawin, Nona S. R., Duarte Carlos M., and Agustí S.: Nutrient and temperature control of the contribution of picoplankton to phytoplankton biomass and production, Limnol. Oceanogr., 45, 591–600, doi:10.4319/lo.2000.45.3.0591, 2000.

Aiken, J., Hardman-Mountford, N. J., Barlow, R., Fishwick, J., Hirata, T., and Smyth, T.: Functional links between bioenergetics and bio-optical traits of phytoplankton taxonomic groups: an overarching hypothesis with applications for ocean colour remote sensing, J. Plankton Res., 30, 165–181, 2008.

Alvain, S., Moulin, C., Dandonneau, Y., and Loisel, H.: Seasonal distribution and succession of dominant phytoplankton groups in the global ocean: a satellite view, Global Biogeochem. Cy., 22, GB3001, doi:10.1029/2007GB003154, 2008.

OSD
12, 573–644, 2015

Amante, C. and Eakins, B. W.: ETOPO1 1 Arc-Minute Global Relief Model: Procedures, Data Sources and Analysis, NOAA Technical Memorandum NESDIS NGDC-24, National Geophysical Data Center, NOAA, doi:10.7289/V5C8276M, last access: 30 January 2015, 2009.
Antoine, D., André, J. M., and Morel, A.: Oceanic primary production. 2. Estimation at global scale from satellite (coastal zone color scanner) chlorophyll, Global Biogeochem. Cy., 10, 57–69, 1996.
Assmann, K. M., Bentsen, M., Segschneider, J., and Heinze, C.: An isopycnic ocean carbon cycle model, Geosci. Model Dev., 3, 143–167, doi:10.5194/gmd-3-143-2010, 2010.
Aumont, O. and Bopp, L.: Globalizing results from ocean in situ iron fertilization studies, Global Biogeochem. Cy., 20, GB2017, doi:10.1029/2005gb002591, 2006.
Ayers, G. P. and Cainey, J. M.: The CLAW hypothesis: a review of the major developments, Environ. Chem., 4, 366–374, 2007.
Behrenfeld, M. J. and Falkowski, P. G.: A consumer's guide to phytoplankton primary productivity models, Limnol. Oceanogr., 42, 1479–1491, 1997a.
Behrenfeld, M. J. and Falkowski, P. G.: Photosynthetic rates derived from satellite-based chlorophyll concentration, Limnol. Oceanogr., 42, 1–20, 1997b.
Behrenfeld, M. J., Boss, E., Siegel, D. A., and Shea, D. M.: Carbon-based ocean productivity and phytoplankton physiology from space, Global Biogeochem. Cy., 19, GB1006, 10.1029/2004GB002299, 2005.
Behrenfeld, M. J., O'Malley, R. T., Siegel, D. A., McClain, C. R., Sarmiento, J. L., Feldman, G. C., Milligan, A. J., Falkowski, P. G., Letelier, R. M., and Boss, E. S.: Climate-driven trends in contemporary ocean productivity, Nature, 444, 752–755, 2006.
Boss, E., Twardowski, M. S., and Herring, S.: The shape of the particulate beam attenuation spectrum and its relation to the size distribution of oceanic particles, Appl. Optics, 40, 4885–4893, 2001.
Bracher, A., Vountas, M., Dinter, T., Burrows, J. P., Röttgers, R., and Peeken, I.: Quantitative observation of cyanobacteria and diatoms from space using PhytoDOAS on SCIAMACHY data, Biogeosciences, 6, 751–764, doi:10.5194/bg-6-751-2009, 2009.
Brewin, R. J. W., Sathyendranath, S., Hirata, T., Lavender, S. J., Barciela, R., and Hardman-Mountford, N. J.: A three-component model of phytoplankton size class for the Atlantic Ocean, Ecol. Model., 221, 1472–1483, 2010.
Brewin, R. J. W., Hardman-Mountford, N. J., Lavender, S. J., Raitsos, D. E., Hirata, T., Uitz, J., Devred, E., Bricaud, A., Ciotti, A., and Gentili, B.: An intercomparison of bio-optical tech-

OSD
12, 573–644, 2015

niques for detecting phytoplankton size class from satellite remote sensing, Remote Sens. Environ., 115, 325–339, 2011.
Cabré, A., Marinov, I., and Leung, S.: Consistent global responses of marine ecosystems to future climate change across the IPCC AR5 earth system models, Clim. Dynam., 1–28, doi:10.1007/s00382-014-2374-3, 2014.
Carr, M.-E., Friedrichs, M. A. M., Schmeltz, M., Aita, M. N., Antoine, D., Arrigo, K. R., Asanuma, I., Aumont, O., Barber, R., Behrenfeld, M., Bidigare, R., Buitenhuis, E. T., Campbell, J., Ciotti, A., Dierssen, H., Dowell, M., Dunne, J., Esaias, W., Gentili, B., Gregg, W., Groom, S., Hoepffner, N., Ishizaka, J., Kameda, T., Le Quéré, C., Lohrenz, S., Marra, J., Mélin, F., Moore, K., Morel, A., Reddy, T. E., Ryan, J., Scardi, M., Smyth, T., Turpie, K., Tilstone, G., Waters, K., and Yamanaka, Y.: A comparison of global estimates of marine primary production from ocean color, Deep-Sea Res. Pt. II, 53, 741–770, doi:10.1016/j.dsr2.2006.01.028, 2006.
Chisholm, S. W.: Phytoplankton Size, in: Primary productivity and biogeochemical cycles in the sea, edited by: Falkowski, P. G. and Woodhead, A. D., Plenum Press, New York, 213–237, 1992.
Ciotti, A. and Bricaud, A.: Retrievals of a size parameter for phytoplankton and spectral light absorption by colored detrital matter from water-leaving radiances at SeaWiFS channels in a continental shelf region off Brazil, Limnol. Oceanogr.-Meth., 4, 237–253, 2006.
Clavano, W. R., Boss, E., and Karp-Boss, L.: Inherent optical properties of non-spherical marine-like particles – from theory to observation, Oceanogr. Mar. Biol., 45, 1–38, 2007.
Dall'Olmo, G., Westberry, T. K., Behrenfeld, M. J., Boss, E., and Slade, W. H.: Significant contribution of large particles to optical backscattering in the open ocean, Biogeosciences, 6, 947–967, doi:10.5194/bg-6-947-2009, 2009.
Davidson, K., Roberts, E. C., and Gilpin, L. C.: The relationship between carbon and biovolume in marine microbial mesocosms under different nutrient regimes, Eur. J. Phycol., 37, 501–507, 2002.
de Boyer Montégut, C., Madec, G., Fischer, A. S., Lazar, A., and Iudicone, D.: Mixed layer depth over the global ocean: An examination of profile data and a profile-based climatology, J. Geophys. Res.-Oceans, 109, C12003, doi:10.1029/2004JC002378, 2004.
Dierssen, H. M. and Smith, R. C.: Bio-optical properties and remote sensing ocean color algorithms for Antarctic Peninsula waters, J. Geophys. Res.-Oceans, 105, 26301–26312, 2000.

OSD
12, 573–644, 2015

Dugdale, R. C. and Wilkerson, F. P.: Low specific nitrate uptake rate: A common feature of high-nutrient, low-chlorophyll marine ecosystems, Limnol. Oceanogr., 36, 1678–1688, 1991.
Dunne, J. P., John, J. G., Shevliakova, E., Stouffer, R. J., Krasting, J. P., Malyshev, S. L., Milly, P. C. D., Sentman, L. T., Adcroft, A. J., Cooke, W., Dunne, K. A., Griffies, S. M., Hallberg, R. W., Harrison, M. J., Levy, H., Wittenberg, A. T., Phillips, P. J., and Zadeh, N.: GFDL's ESM2 global coupled climate–carbon Earth system models. Part II: Carbon system formulation and baseline simulation characteristics, J. Climate, 26, 2247–2267, doi:10.1175/jcli-d-12-00150.1, 2013.
DuRand, M. D., Olson, R. J., and Chisholm, S. W.: Phytoplankton population dynamics at the Bermuda Atlantic Time-series station in the Sargasso Sea, Deep-Sea Res. Pt. II, 48, 1983–2003, 2001.
Eppley, R. W. and Peterson, B. J.: Particulate organic matter flux and planktonic new production in the deep ocean, Nature, 282, 677–680, 1979.
Eppley, R. W., Chavez, F. P., and Barber, R. T.: Standing stocks of particulate carbon and nitrogen in the equatorial Pacific at 150° W, J. Geophys. Res.-Oceans, 97, 655–661, 1992.
Falkowski, P. G. and Oliver, M. J.: Mix and match: how climate selects phytoplankton, Nat. Rev. Microbiol., 5, 813–819, 2007.
Falkowski, P. G., Barber, R. T., and Smetacek, V.: Biogeochemical controls and feedbacks on ocean primary production, Science, 281, 200–206, 1998.
Fay, A. R. and McKinley, G. A.: Global open-ocean biomes: mean and temporal variability, Earth Syst. Sci. Data, 6, 273–284, doi:10.5194/essd-6-273-2014, 2014.
Field, C. B., Behrenfeld, M. J., Randerson, J. T., and Falkowski, P.: Primary production of the biosphere: integrating terrestrial and oceanic components, Science, 281, 237–240, 1998.
Frouin, R. and Iacobellis, S. F.: Influence of phytoplankton on the global radiation budget, J. Geophys. Res.-Atmos., 107, ACL-5, 2002.
Fujiwara, A., Hirawake, T., Suzuki, K., and Saitoh, S.-I.: Remote sensing of size structure of phytoplankton communities using optical properties of the Chukchi and Bering Sea shelf region, Biogeosciences, 8, 3567–3580, doi:10.5194/bg-8-3567-2011, 2011.
Garcia, C. A. E., Garcia, V. M. T., and McClain, C. R.: Evaluation of SeaWiFS chlorophyll algorithms in the Southwestern Atlantic and Southern Oceans, Remote Sens. Environ., 95, 125–137, 2005.

OSD
12, 573–644, 2015

Garver, S. A. and Siegel, D. A.: Inherent optical property inversion of ocean color spectra and its biogeochemical interpretation. 1. Time series from the Sargasso Sea, J. Geophys. Res.-Oceans, 102, 18607–18625, 1997.
Geider, R. J.: Light and temperature dependence of the carbon to chlorophyll *a* ratio in microalgae and cyanobacteria: implications for physiology and growth of phytoplankton, New Phytol., 106, 1–34, 1987.
Geider, R. J., MacIntyre, H. L., and Kana, T. M.: A dynamic regulatory model of phytoplanktonic acclimation to light, nutrients, and temperature, Limnol. Oceanogr., 43, 679–694, 1998.
Graff, J. R., Milligan, A. J., and Behrenfeld, M. J.: The measurement of phytoplankton biomass using flow-cytometric sorting and elemental analysis of carbon, Limnol. Oceanogr.-Meth., 10, 910–920, 2012.
Gregg, W. W.: Assimilation of SeaWiFS ocean chlorophyll data into a three-dimensional global ocean model, J. Marine Syst., 69, 205–225, doi:10.1016/j.jmarsys.2006.02.015, 2008.
Gregg, W. W., Casey, N. W., O'Reilly, J. E., and Esaias, W. E.: An empirical approach to ocean color data: reducing bias and the need for post-launch radiometric re-calibration, Remote Sens. Environ., 113, 1598–1612, 2009.
Gundersen, K., Orcutt, K. M., Purdie, D. A., Michaels, A. F., and Knap, A. H.: Particulate organic carbon mass distribution at the Bermuda Atlantic Time-series Study (BATS) site, Deep-Sea Res. Pt. II, 48, 1697–1718, 2001.
Hirata, T.: Satellite Phytoplankton Functional Type Algorithm Intercomparison Project, available at: http://pft.ees.hokudai.ac.jp/satellite/index.shtml (last access: 11 March 2015), 2015.
Hirata, T., Hardman-Mountford, N. J., Brewin, R. J. W., Aiken, J., Barlow, R., Suzuki, K., Isada, T., Howell, E., Hashioka, T., Noguchi-Aita, M., and Yamanaka, Y.: Synoptic relationships between surface Chlorophyll-*a* and diagnostic pigments specific to phytoplankton functional types, Biogeosciences, 8, 311–327, doi:10.5194/bg-8-311-2011, 2011.
Hirata, T., Hardman-Mountford, N., and Brewin, R. J. W.: Comparing satellite-based phytoplankton classification methods, EOS Trans. AGU, 93, 2012.
Hood, R. R., Laws, E. A., Armstrong, R. A., Bates, N. R., Brown, C. W., Carlson, C. A., Chai, F., Doney, S. C., Falkowski, P. G., Feely, R. A., Friedrichs, M. A. M., Landry, M. R., Moore, J. K., Nelson, D. M., Richardson, T. L., Salihoglu, B., Schartau, M., Toole, D. A., and Wiggert, J. D.: Pelagic functional group modeling: Progress, challenges and prospects, Deep-Sea Res. Pt. II, 53, 459–512, 2006.

OSD
12, 573–644, 2015

Ilyina, T., Six, K. D., Segschneider, J., Maier-Reimer, E., Li, H. M., and Nunez-Riboni, I.: Global ocean biogeochemistry model HAMOCC: model architecture and performance as component of the MPI-Earth system model in different CMIP5 experimental realizations, J. Adv. Model. Earth Syst., 5, 287–315, doi:10.1029/2012ms000178, 2013.

Ingleby, B. and Huddleston, M.: Quality control of ocean temperature and salinity profiles – historical and real-time data, J. Marine Syst., 65, 158–175, 2007.

IOCCG: Phytoplankton Functional Types from Space, edited by: Sathyendranath, S., Reports of the International Ocean-Colour Coordinating Group, No. 15, IOCCG, Dartmouth, Canada, 2014.

IPCC: Climate Change 2013: the Physical Science Basis, Contribution of Working Group I to the Fifth Assessment Report of the Intergovernmental Panel on Climate Change, edited by: Stocker, T. F., Qin, D., Plattner, G.-K., Tignor, M., Allen, S. K., Boschung, J., Nauels, A., Xia, Y., Bex, V., and Midgley, P. M., Cambridge University Press, Cambridge, UK and New York, NY, USA, 1535 pp., doi:10.1017/CBO9781107415324, 2013.

Jennings, B. R. and Parslow, K.: Particle size measurement: the equivalent spherical diameter, P. Roy. Soc. Lond. A Math., 419, 137–149, 1988.

Junge, C. E.: Air Chemistry and Radioactivity, Academic Press Inc., New York and London, 382 pp., 1963.

Kahru, M. and Mitchell, B. G.: Blending of ocean colour algorithms applied to the Southern Ocean, Remote Sens. Lett., 1, 119–124, 2010.

Kostadinov, T. S.: Satellite Retrieval of Phytoplankton Functional Types and Carbon via the Particle Size Distribution, Ph.D. thesis, University of California, Santa Barbara, 2009.

Kostadinov, T. S., Siegel, D. A., Maritorena, S., and Guillocheau, N.: Ocean color observations and modeling for an optically complex site: Santa Barbara Channel, California, USA, J. Geophys. Res., 112, C07011, doi:10.1029/2006JC003526, 2007.

Kostadinov, T. S., Siegel, D. A., and Maritorena, S.: Retrieval of the particle size distribution from satellite ocean color observations, J. Geophys. Res.-Oceans, 114, C09015, doi:10.1029/2009JC005303, 2009.

Kostadinov, T. S., Siegel, D. A., and Maritorena, S.: Global variability of phytoplankton functional types from space: assessment via the particle size distribution, Biogeosciences, 7, 3239–3257, doi:10.5194/bg-7-3239-2010, 2010.

OSD
12, 573–644, 2015

Kostadinov, T. S., Siegel, D. A., Maritorena, S., and Guillocheau, N.: Optical assessment of particle size and composition in the Santa Barbara Channel, California, Appl. Optics, 51, 3171–3189, 2012.

Ku, H. H.: Notes on the use of propagation of error formulas, J. Res. NBS. C Eng. Inst., 70, 263–273, 1966.

Landry, M. R., Ondrusek, M. E., Tanner, S. J., Brown, S. L., Constantinou, J., Bidigare, R. R., Coale, K. H., and Fitzwater, S.: Biological response to iron fertilization in the eastern equatorial Pacific (IronEx II). I. Microplankton community abundances and biomass, Mar. Ecol.-Prog. Ser., 201, 27–42, 2000.

Le Quéré, C., Aumont, O., Monfray, P., and Orr, J.: Propagation of climatic events on ocean stratification, marine biology, and CO_2: case studies over the 1979–1999 period, J. Geophys. Res., 108, 3375, doi:10.1029/2001JC000920, 2003.

Le Quéré, C., Harrison, S. P., Prentice, I. C., Buitenhuis, E. T., Aumont, O., Bopp, L., Claustre, H., Cunha, L. C. D., Geider, R., Giraud, X., Klaas, C., Kohfeld, K. E., Legendre, L., Manizza, M., Platt, T., Rivkin, R. B., Sathyendranath, S., Uitz, J., Watson, A. J., and Wolf-Gladrow, D.: Ecosystem dynamics based on plankton functional types for global ocean biogeochemistry models, Glob. Change Biol., 11, 2016–2040, 2005.

Levitus, S.: Climatological Atlas of the World Ocean, US Department of Commerce, National Oceanic and Atmospheric Administration, Rockville, MD, 190 pp., 1982.

Loisel, H. and Stramski, D.: Estimation of the inherent optical properties of natural waters from irradiance attenuation coefficient and reflectance in the presence of Raman scattering, Appl. Optics, 39, 3001–3011, 2000.

Loisel, H., Nicolas, J.-M., Sciandra, A., Stramski, D., and Poteau, A.: Spectral dependency of optical backscattering by marine particles from satellite remote sensing of the global ocean, J. Geophys. Res., 111, C09024, doi:10.1029/2005JC003367, 2006.

Longhurst, A. R.: Ecological Geography of the Sea, 2nd edn., Academic Press, Burlington, 560 pp., 2007.

Marinov, I., Follows, M., Gnanadesikan, A., Sarmiento, J. L., and Slater, R. D.: How does ocean biology affect atmospheric pCO_2? Theory and models, J. Geophys. Res.-Oceans, 13, C07032, doi:10.1029/2007JC004598, 2008.

Marinov, I., Doney, S., Lima, I., Lindsey, K., Moore, K., and Mahowald, N.: North–South asymmetry in the modeled phytoplankton community response to climate change over the 21st century, Global Biogeochem. Cy., 27, 1274–1290, doi:10.1002/2013GB004599, 2013.

OSD
12, 573–644, 2015

Maritorena, S., Siegel, D. A., and Peterson, A. R.: Optimization of a semianalytical ocean color model for global-scale applications, Appl. Optics, 41, 2705–2714, 2002.
Maritorena, S., d'Andon, O. H. F., Mangin, A., and Siegel, D. A.: Merged satellite ocean color data products using a bio-optical model: characteristics, benefits and issues, Remote Sens. Environ., 114, 1791–1804, 2010.
Martinez-Vicente, V., Dall'Olmo, G., Tarran, G., Boss, E., and Sathyendranath, S.: Optical backscattering is correlated with phytoplankton carbon across the Atlantic Ocean, Geophys. Res. Lett., 40, 1154–1158, doi:10.1002/grl.50252, 2013.
McClain, C. R.: A decade of satellite ocean color observations, Ann. Rev. Mar. Sci., 1, 19–42, 2009.
Menden-Deuer, S. and Lessard, E.: Carbon to volume relationships for dinoflagellates, diatoms, and other protist plankton, Limnol. Oceanogr., 45, 569–579, 2000.
Mie, G.: Beiträge zur Optik trüber Medien, speziell kolloidaler Metallösungen, Ann. Phys., 330, 377–445, 1908.
Milutinović, S. and Bertino, L.: Assessment and propagation of uncertainties in input terms through an ocean-colour-based model of primary productivity, Remote Sens. Environ., 115, 1906–1917, 2011.
Moal, J., Martin-Jezequel, V., Harris, R. P., Samain, J. F., and Poulet, S. A.: Interspecific and intraspecific variability of the chemical composition of marine phytoplankton, Oceanol. Acta, 10, 339–346, 1987.
Moberg, E. A. and Sosik, H. M.: Distance maps to estimate cell volume from two-dimensional plankton images, Limnol. Oceanogr.-Meth., 10, 278–288, 2012.
Moore, J. K., Doney, S. C., Lindsay, K.: Upper ocean ecosystem dynamics and iron cycling in a global three-dimensional model, Global Biogeochem. Cy., 18, GB4028, doi:10.1029/2004gb002220, 2004.
Moore, J. K., Doney, S. C., Lindsay, K., Mahowald, N., and Michaels, A. F.: Nitrogen fixation amplifies the ocean biogeochemical response to decadal timescale variations in mineral dust deposition, Tellus B, 58, 560–572, doi:10.1111/j.1600-0889.2006.00209.x, 2006.
Morel, A. and Berthon, J. F.: Surface pigments, algal biomass profiles, and potential production of the euphotic layer – relationships reinvestigated in view of remote-sensing applications, Limnol. Oceanogr., 34, 1545–1562, 1989.

OSD
12, 573–644, 2015

Mouw, C. B. and Yoder, J. A.: Optical determination of phytoplankton size composition from global SeaWiFS imagery, J. Geophys. Res.-Oceans, 115, C12018, doi:10.1029/2010JC006337, 2010.
Nair, A., Sathyendranath, S., Platt, T., Morales, J., Stuart, V., Forget, M. H., Devred, E., and Bouman, H.: Remote sensing of phytoplankton functional types, Remote Sens. Environ., 112, 3366–3375, 2008.
Neukermans, G., Loisel, H., Mériaux, X., Astoreca, R., and McKee, D.: In situ variability of mass-specific beam attenuation and backscattering of marine particles with respect to particle size, density, and composition, Limnol. Oceanogr., 57, 124–144, doi:10.4319/lo.2012.57.1.0124, 2012.
O'Reilly, J. E., Maritorena, S., Mitchell, B. G., Siegel, D. A., Carder, K. L., Garver, S. A., Kahru, M., and McClain, C. R.: Ocean color chlorophyll algorithms for SeaWiFS, J. Geophys. Res., 103, 24937–24953, 1998.
O'Reilly, J. E., Siegel, D. A., J. Mueller and 22 Coauthors: SeaWiFS Postlaunch Calibration and Validation Analyses, Part 3, NASA Tech. Memo., 2000-206892, vol. 11, edited by: Hooker, S. B. and Firestone, E. R., NASA Goddard Space Flight Center, 49 pp., 2000.
Otero, M. and Siegel, D. A.: Spatial and temporal characteristics of sediment plumes and phytoplankton blooms in the Santa Barbara Channel, Deep-Sea Res. Pt. II, 51, 1129–1149, 2004.
Oubelkheir, K. J., Claustre, H., Sciandra, A., and Babin, M.: Bio-optical and biogeochemical properties of different trophic regimes in oceanic waters, Limnol. Oceanogr., 50, 1795–1809, 2005.
Palmer, J. R. and Totterdell, I. J.: Production and export in a global ocean ecosystem model, Deep-Sea Res. Pt. I, 48, 1169–1198, doi:10.1016/s0967-0637(00)00080-7, 2001.
Partensky, F., Hess, W. R., and Vaulot, D.: Prochlorococcus, a marine photosynthetic prokaryote of global significance, Microbiol. Mol. Biol. R., 63, 106–127, 1999.
Pérez, V., Fernandez, E., Marañón, E., Moran, X. A. G., and Zubkov, M. V.: Vertical distribution of phytoplankton biomass, production and growth in the Atlantic subtropical gyres, Deep-Sea Res. Pt. I, 53, 1616–1634, 2006.
Quirantes, A. and Bernard, S.: Light scattering by marine algae: two-layer spherical and non-spherical models, J. Quant. Spectrosc. Ra., 89, 311–321, 2004.

OSD
12, 573–644, 2015

Raitsos, D. E., Lavender, S. J., Maravelias, C. D., Haralabous, J., Richardson, A. J., and Reid, P.: Identifying four phytoplankton functional types from space: an ecological approach, Limnol. Oceanogr., 53, 605–613, 2008.
Raven, J. A.: The twelfth tansley lecture, small is beautiful: the picophytoplankton, Funct. Ecol., 12, 503–513, 1998.
Reynolds, R. A., Stramski, D., Wright, V. M., and Woźniak, S. B.: Measurements and characterization of particle size distributions in coastal waters, J. Geophys. Res., 115, C08024, doi:10.1029/2009JC005930, 2010.
Roy, S., Sathyendranath, S., Bouman, H., and Platt, T.: The global distribution of phytoplankton size spectrum and size classes from their light-absorption spectra derived from satellite data, Remote Sens. Environ., 139, 185–197, 2013.
Sathyendranath, S.: General introduction, in: Remote Sensing of Ocean Colour in Coastal, and Other Optically-Complex, Waters, edited by: Sathyendranath, S., International Ocean-Colour Coordinating Group, Dartmouth, Canada, 5–21, 2000.
Sathyendranath, S., Stuart, V., Nair, A., Oka, K., Nakane, T., Bouman, H., Forget, M. H., Maass, H., and Platt, T.: Carbon-to-chlorophyll ratio and growth rate of phytoplankton in the sea, Mar. Ecol.-Prog. Ser., 383, 73–84, 2009.
Seferian, R., Bopp, L., Gehlen, M., Orr, J. C., Ethé, C., Cadule, P., Aumont, O., Salas y Mélia, D., Voldoire, A., and Madec, G.: Skill assessment of three earth system models with common marine biogeochemistry, Clim. Dynam., 40, 2549–2573, doi:10.1007/s00382-012-1362-8, 2013.
Sieburth, J. M., Smetacek, V., and Lenz, J.: Pelagic ecosystem structure: heterotrophic compartments of the plankton and their relationship to plankton size fractions, Limnol. Oceanogr., 23, 1256–1263, 1978.
Siegel, D. A., Maritorena, S., Nelson, N. B., and Behrenfeld, M. J.: Independence and interdependencies among global ocean color properties: reassessing the bio-optical assumption, J. Geophys. Res., 110, C07011, doi:10.1029/2004JC002527, 2005.
Siegel, D. A., Behrenfeld, M. J., Maritorena, S., McClain, C. R., Antoine, D., Bailey, S. W., Bontempi, P. S., Boss, E. S., Dierssen, H. M., Doney, S. C., Eplee Jr, R. E., Evans, R. H., Feldman, G. C., Fields, E., Franz, B. A., Kuring, N. A., Mengelt, C., Nelson, N. B., Patt, F. S., Robinson, W. D., Sarmiento, J. L., Swan, C. M., Werdell, P. J., Westberry, T. K., Wilding, J. G., and Yoder, J. A.: Regional to global assessments of phytoplankton dynamics from the SeaWiFS mission, Remote Sens. Environ., 135, 77–91, 2013.

OSD
12, 573–644, 2015

Smith, R. C. and Baker, K. S.: Optical classification of natural waters, Limnol. Oceanogr., 23, 260–267, 1978.
Stramski, D.: Refractive index of planktonic cells as a measure of cellular carbon and chlorophyll a content, Deep-Sea Res. Pt. I, 46, 335–351, 1999.
Stramski, D. and Kiefer, D. A.: Light scattering by microorganisms in the open ocean, Prog. Oceanogr., 28, 343–383, 1991.
Stramski, D., Shalapyonok, A., and Reynolds, R. A.: Optical characterization of the oceanic unicellular cyanobacterium Synechococcus grown under a day-night cycle in natural irradiance, J. Geophys. Res., 100, 13295–13307, doi:10.1029/95JC00452, 1995.
Stramski, D., Boss, E., Bogucki, D., and Voss, K. J.: The role of seawater constituents in light backscattering in the ocean, Prog. Oceanogr., 61, 27–55, 2004.
Stramski, D., Reynolds, R. A., Babin, M., Kaczmarek, S., Lewis, M. R., Röttgers, R., Sciandra, A., Stramska, M., Twardowski, M. S., Franz, B. A., and Claustre, H.: Relationships between the surface concentration of particulate organic carbon and optical properties in the eastern South Pacific and eastern Atlantic Oceans, Biogeosciences, 5, 171–201, doi:10.5194/bg-5-171-2008, 2008.
Taylor, K. E., Stouffer, R. J., and Meehl, G. A.: An overview of CMIP5 and the experiment design, B. Am. Meteorol. Soc., 93, 485–498, doi:10.1175/bams-d-11-00094.1, 2012.
Toole, D. A. and Siegel, D. A.: Modes and mechanisms of ocean color variability in the Santa Barbara Channel, J. Geophys. Res., 160, 26985–27000, 2001.
Uitz, J., Claustre, H., Morel, A., and Hooker, S. B.: Vertical distribution of phytoplankton communities in open ocean: an assessment based on surface chlorophyll, J. Geophys. Res.-Oceans, 111, C08005, doi:10.1029/2005JC003207, 2006.
Uitz, J., Claustre, H., Gentili, B., and Stramski, D.: Phytoplankton class-specific primary production in the world's oceans: seasonal and interannual variability from satellite observations, Global Biogeochem. Cy., 24, GB3016, doi:10.1029/2009GB003680, 2010.
UNESCO, ICES, SCOR, and IAPSO: Tenth Report of the Joint Panel on Oceanographic Tables and Standards, UNESCO, Sidney, BC, Canada, 25 pp., 1980.
Vallina, S. M. and Simó, R.: Strong relationship between DMS and the solar radiation dose over the global surface ocean, Science, 315, 506–508, 2007.
Vidussi, F., Claustre, H., Manca, B. B., Luchetta, A., and Marty, J. C.: Phytoplankton pigment distribution in relation to upper thermocline circulation in the eastern Mediterranean Sea during winter, J. Geophys. Res., 106, 19939–19956, 2001.

OSD
12, 573–644, 2015

Verity, P. G., Robertson, C. Y., Tronzo, C. R., Andrews, M. G., Nelson, J. R., and Sieracki, M. E.: Relationships between cell volume and the carbon and nitrogen content of marine photosynthetic nanoplankton, Limnol. Oceanogr., 37, 1434–1446, 1992.

Wessel, P. and Smith, W. H. F. A.: Global self-consistent, hierarchical, high-resolution shoreline database, J. Geophys. Res., 101, 8741–8743, 1996.

Westberry, T., Behrenfeld, M. J., Siegel, D. A., and Boss, E.: Carbon-based primary productivity modeling with vertically resolved photoacclimation, Global Biogeochem. Cy., 22, GB2024, doi:10.1029/2007GB003078, 2008.

Wieser, M. E., Holden, N., Coplen, T. B., Böhlke, J. K., Berglund, M., Brand, W. A., De Bièvre, P., Gröning, M., Loss, R. D., Meija, J., Hirata, T., Prohaska, T., Schoenberg, R., O'Connor, G., Walczyk, T., Yoneda, S., and Zhu, X. K.: Atomic weights of the elements 2011 (IUPAC Technical Report), Pure Appl. Chem., 85, 1047–1078, 2013.

Wozniak, S. B. and Stramski, D.: Modeling the optical properties of mineral particles suspended in seawater and their influence on ocean reflectance and chlorophyll estimation from remote sensing algorithms, Appl. Optics, 43, 3489–3503, 2004.

Yukimoto, S., Yoshimura, H., Hosaka, M., Sakami, T., Tsujino, H., Hirabara, M., Tanaka, T. Y., Deushi, M., Obata, A., Nakano, H., Adachi,Y., Shindo, E., Yabu, S.: Tomoaki Ose and Akio Kitoh: Meteorological Research Institute-Earth System Model Version 1 (MRI-ESM1) – Model Description, Meteorological Reports of the Meteorological Research Institute, 64 pp., 2011.

Zahariev, K., Christian, J. R., and Denman, K. L.: Preindustrial, historical, and fertilization simulations using a global ocean carbon model with new parameterizations of iron limitation, calcification, and N-2 fixation, Prog. Oceanogr., 77, 56–82, doi:10.1016/j.pocean.2008.01.007, 2008.

OSD
12, 573–644, 2015

Table 1a. The values of parameters a and b in the allometric Eq. (3), as used in Eq. (5) in this study to convert volume to carbon. Coefficient values are from Menden-Deuer and Lessard (2000), their Table 4. Standard deviation of the regression coefficients are given in parentheses. The applicable diameter range for each allometric relationship and the weights applied to it (Eq. 5) are also given. V_{cell} stands for cellular volume.

Coefficient set # (i)	Phytoplankton group	log10(a) (σ)	b (σ)	Diameter range applied to [µm]	Weight w_i (Eq. 5)
1	$V^*_{cell} < 3000\,\mu m^3$	−0.583 (0.080)	0.860 (0.030)	0.5–17.894	1
2	All except diatoms	−0.665 (0.066)	0.939 (0.021)	17.894–50	0.5
3	Diatoms with $V_{cell} > 3000\,\mu m^3$	−0.933 (0.226)	0.881 (0.045)	17.894–50	0.5

OSD
12, 573–644, 2015

Table 1b. Size limits of integration (cellular diameter in µm) applied to the three allometric relationships in Table 1a for the computation of carbon biomass in each size class. These are the D_{min} and D_{max} values used in Eq. (5), with the corresponding weights w_i (Table 1a). The allometric coefficients sets correspond to index i in Eqs. (5) and (6). The resulting net volume to carbon relationship used in this study is plotted in Fig. 1.

Size Class/Allometric Coefficient Set Index i	$i = 1$	$i = 2$	$i = 3$
Picoplankton	0.5–2	–	–
Nanoplankton	2–17.894	17.894–20	17.894–20
Microplankton	–	20–50	20–50
Total C biomass	0.5–17.894	17.894–50	17.894–50

OSD
12, 573–644, 2015

Table 2. Summary of the CMIP5 models that include phytoplankton biomass and primary production. The table includes: spatial resolution in the atmosphere and ocean, list of nutrient tracers, ecology subroutine, phytoplankton functional groups modelled, references, and weight we applied in the inter-model averages.

Model	Nutrients	Ecology module	Phytoplankton variables	References	Weight
CanESM2	N, (but also accounts for Fe limitation)	NPZD based on Denman and Peña (1999).	Generic phytoplankton	Zahariev et al. (2008)	1
CESM1-BGC	P, N, Fe, Si	MET	Diatoms, small phytoplankton, diazotrophs	Moore et al. (2004, 2006)	1
GFDL-ESM2G (M)	P, N, Fe, Si	TOPAZ2	Large phytoplankton (diatoms, greens, and other large eukaryotes), small phytoplankton (prokaryotic picoplankton and nanoplankton), and diazotrophs	Dunne et al. (2013)	1 (1)
HadGEM2-ES (CC)	N, Fe, Si	Diat-HadOCC (NPZD)	Diatoms, non-diatoms	Palmer and Totterdell (2001)	0.5 (0.5)
IPSL-CM5A-MR (LR)	P, N, Fe, Si	PISCES (from HAMOCC5)	Diatoms, nanophytoplankton (non-diatom). Diatoms differ from nanophytoplankton because they need silicon and more iron and because they have higher half-saturation constants due to their larger mean size.	Aumont and Bopp (2006), Séférian et al. (2013)	0.5 (0.5)
MPI-ESM-MR (LR)	P, N, Fe, Si	HAMOCC5.2 (NPZD)	Generic phytoplankton (Plankton concentration is then subdivided into opal – and calcium carbonate-producing fractions as basis for shell production)	Ilyina et al. (2013)	0.5 (0.5)
MRI-ESM1	P, N	NPZD (Oschiles, 2001)	Generic phytoplankton	Yukimoto et al. (2011)	1
NorESM1-ME	P, N, Fe, Si	HAMOCC5.1 (NPZD)	Generic phytoplankton (Plankton concentration is then subdivided into opal – and calcium carbonate-producing fractions as basis for shell production)	Assmann et al. (2010)	1
GISS-E2-H-CC (GISS-E2-R-CC)	N, Fe, Si	NOBM	Diatoms, chlorophytes, cyanobacteria, coccolitophores	Gregg (2008)	1 (1)

OSD
12, 573–644, 2015

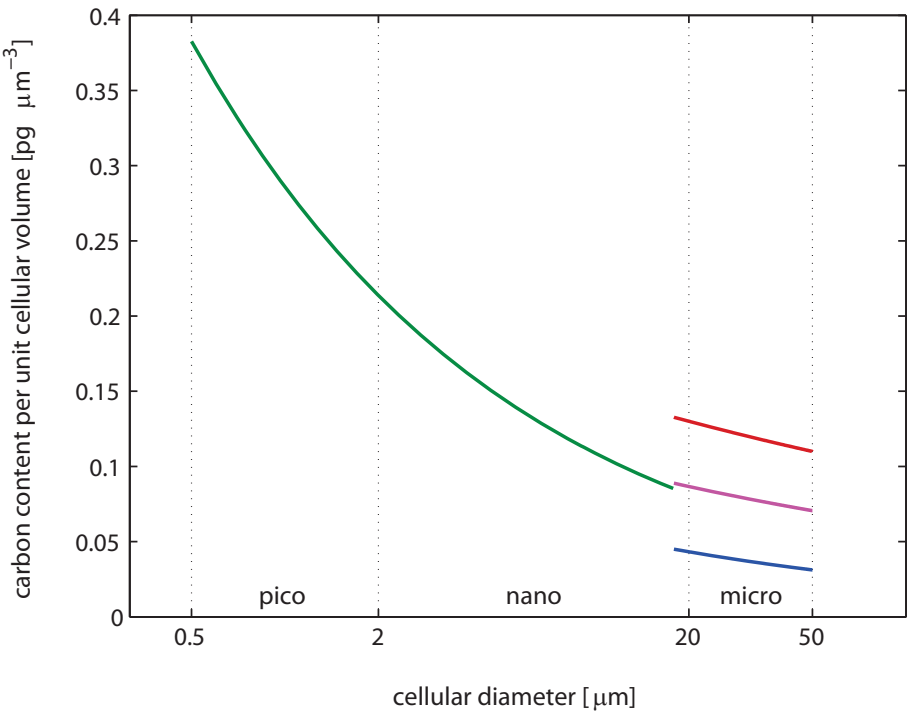

Figure 1. The allometric relationships of Menden-Deuer and Lessard (2000) (MDL2000) (their Table 4) as applied for the carbon biomass algorithm (Sect. 2.1 and Table 1a and b). Carbon content per unit cellular volume is given as a function of cellular diameter. The vertical dotted lines indicate the size ranges of the three phytoplankton size classes (PSCs). The curve exhibits a discontinuity at a diameter of 17.894 μm (V = 3000 μm^3), because different relationships were reported for phytoplankton below and above that size, respectively. For cells larger than this cutoff diameter, two separate allometric relationships are used (diatoms (blue) and all the rest (red)) and averaged (magenta) for use in the operational algorithm.

OSD
12, 573–644, 2015

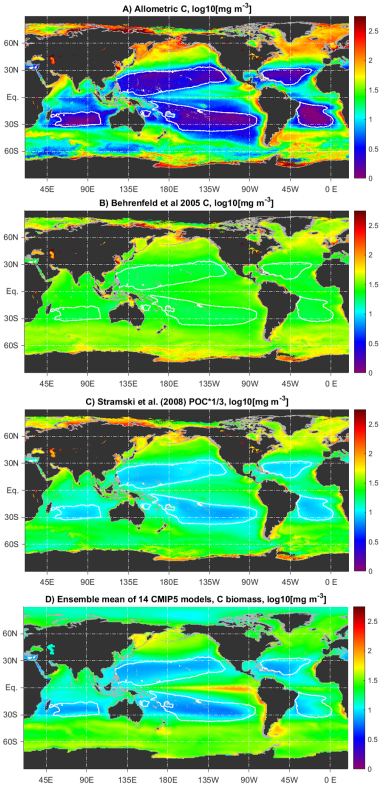

Figure 2. SeaWiFS mission composite mean (September 1997–December 2010) of total phytoplankton carbon biomass ($mg\,m^{-3}$ in log10 space), derived from monthly data using **(a)** the allometric PSD method presented here, **(b)** the method of Behrenfeld et al. (2005) and **(c)** the Stramski et al. (2008) POC retrieval, multiplied by 1/3. **(d)** Ensemble mean of the CMIP5 models' (Table 1a) climatologies (1990–2010) of the surface phytoplankton carbon biomass ($mg\,m^{-3}$). The white contours are the $0.08\,mg\,m^{-3}$ isoline of Chl. Both model and satellite composite means are computed from monthly data in linear space.

OSD
12, 573–644, 2015

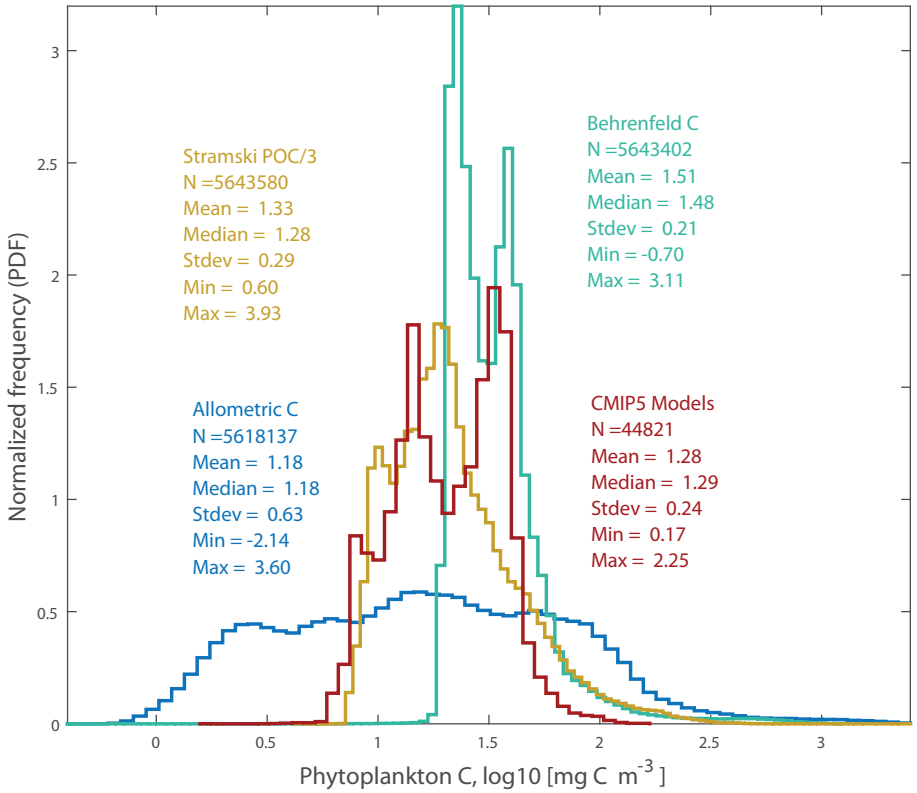

Figure 3. Normalized frequency distributions (probability density functions) of the mission mean phytoplankton carbon biomass images of as in Fig. 2a–d, namely the allometric PSD carbon estimate (light blue), the Stramksi et al. (2008) POC retrieval, multiplied by 1/3 (beige), the Behrenfeld et al. (2005) method (light green), and the ensemble mean of the CMIP5 models (dark red). The *x* axis is in log10-space.

OSD
12, 573–644, 2015

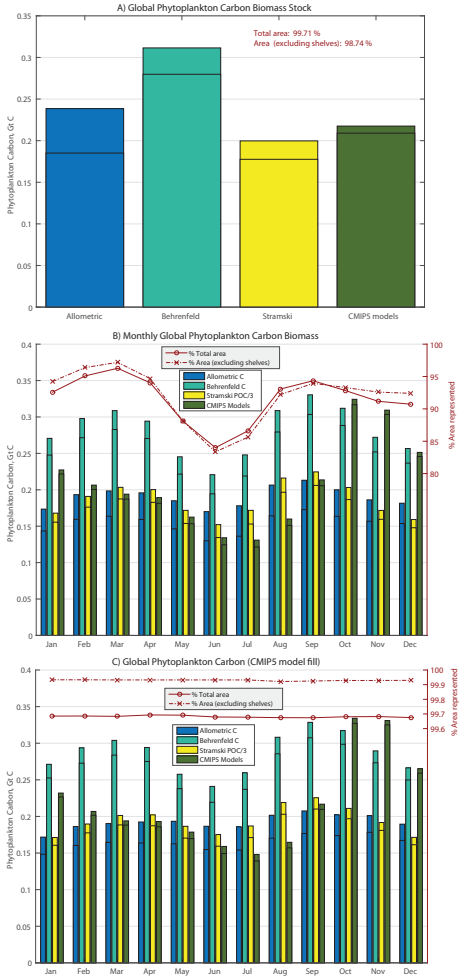

OSD
12, 573–644, 2015

Carbon-based phytoplankton size classes retrieved via the PSD

T. S. Kostadinov et al.

Figure 4. (a) Global spatially integrated mixed layer phytoplankton carbon biomass stock (Gt C), as estimated with three different satellite algorithms (as in Figs. 2a–c and 3) from the SeaWiFS mission composite, and from the CMIP5 model ensemble mean (Fig. 2d), using the same climatological MLD estimate for all estimates. These values were derived using only those pixels (at 1° resolution) where none of the datasets (MLD, satellite-derived, or CMIP5-based) was missing data. **(b)** Same as in **(a)**, but for the monthly composite means for the three satellite data sets and the CMIP5 model ensemble mean. **(c)** Same as in **(b)**, but with missing SeaWiFS pixels gap filled with CMIP5 model data in order to represent the entire ocean in the calculation. Horizontal black lines within each bar on all panels represent the estimate when continental shelves (< 200 m depth) are excluded. The sum of the areas of valid pixels used in the estimates is given as a percentage of total ocean area (3.608×10^8 km^2), and area excluding the shelves ($\sim 3.4 \times 10^8$ km^2), respectively. Areas were estimated from the 1° ETOPO1-based bathymetry; total ocean area is in close agreement with the 3.619×10^8 km^2 estimate of Eakins and Sharman (2010). The carbon biomass and area calculations exclude the Caspian Sea and other major lake bodies.

OSD
12, 573–644, 2015

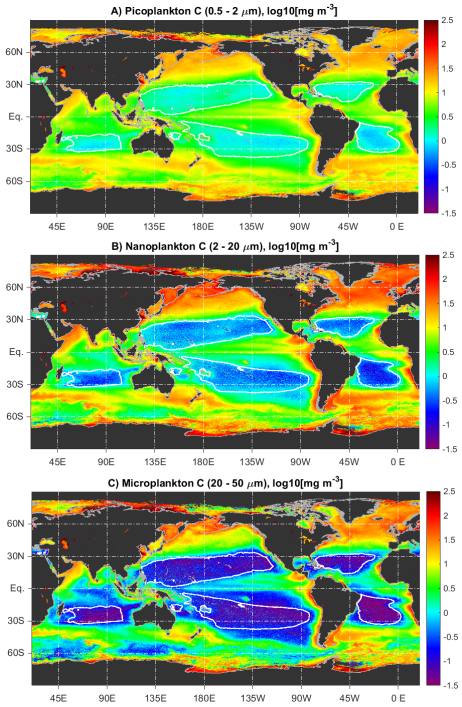

Figure 5. SeaWiFS mission composite (September 1997–December 2010) of size-partitioned phytoplankton carbon biomass, C ($mg\,m^{-3}$ in log10 space) for **(a)** picoplankton, **(b)** nanoplankton and **(c)** microplankton. Carbon biomass in each fraction was estimated using the KSM09 algorithm PSD retrievals to estimate biovolume, which was converted to carbon using the MDL2000 allometric relationships. The white contours are the 0.08 $mg\,m^{-3}$ isoline of Chl. Note that the color scale is different from that of Fig. 2.

OSD
12, 573–644, 2015

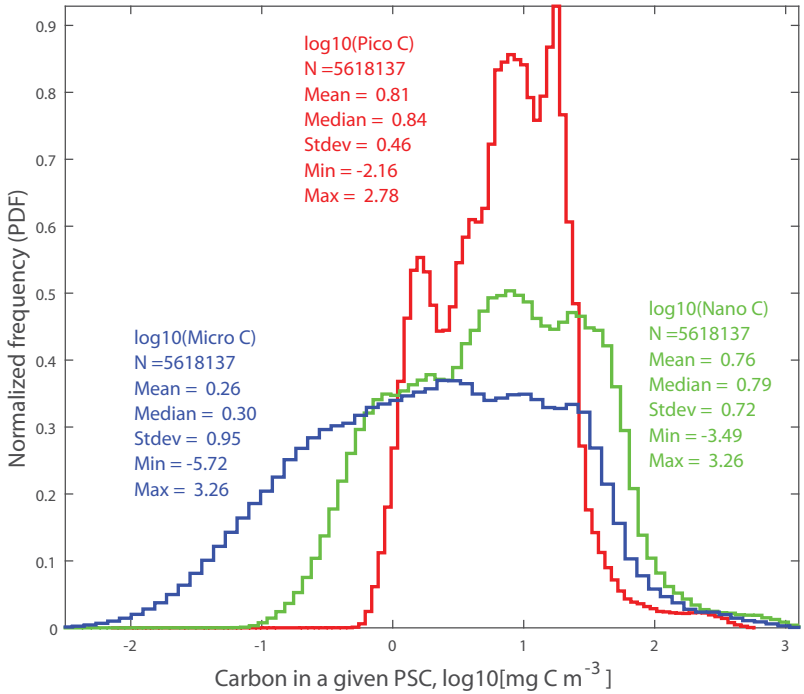

Figure 6. Normalized frequency distributions (probability density functions) computed from the mapped global mission composites of phytoplankton carbon biomass (in log-10 space) in the three PSCs (Fig. 5a–c) – picoplankton (red), nanoplankton (green) and microplankton (blue).

OSD
12, 573–644, 2015

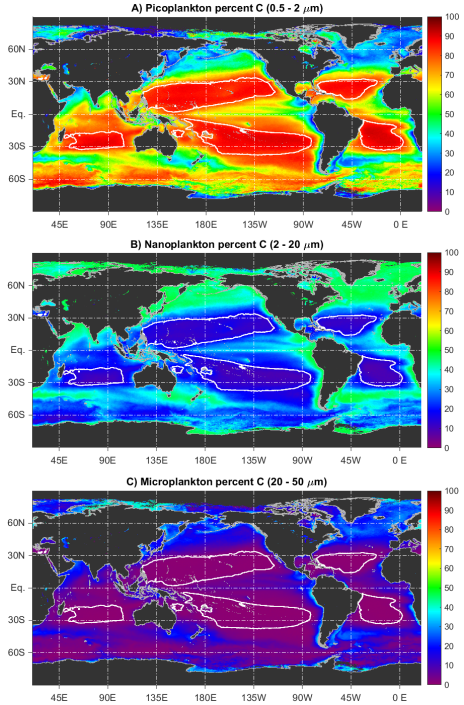

Figure 7. SeaWiFS mission composite (September 1997–December 2010) of percentage contributions of three PSCs to total phytoplankton carbon biomass: **(a)** picoplankton, **(b)** nanoplankton and **(c)** microplankton. This mission composite is computed by averaging the fractional contributions to C biomass for each available month (Fig. A2). The white contours are the 0.08 mg m^{-3} isoline of Chl.

OSD
12, 573–644, 2015

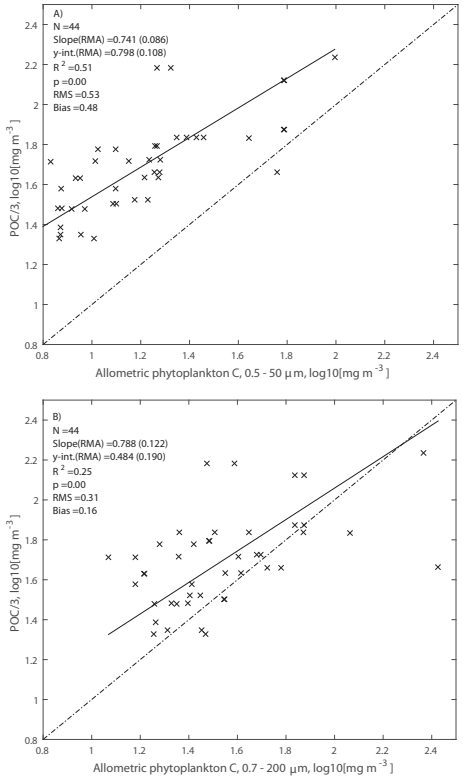

Figure 8. Match-ups between phytoplankton carbon estimated by applying allometric relationships to in-situ measurements of the PSD (x axis) and by multiplying chemical POC determinations by 1/3 (y axis). Measurements are coincident in time and space and were conducted on AMT cruises 2, 3, and 4. Two different limits of integration are used for the allometric estimate: **(a)** 0.5–50 µm, as in the operational satellite algorithm presented here, and **(b)** 0.7–200 µm, matching the GF/F filter pore size used in POC measurements.

OSD
12, 573–644, 2015

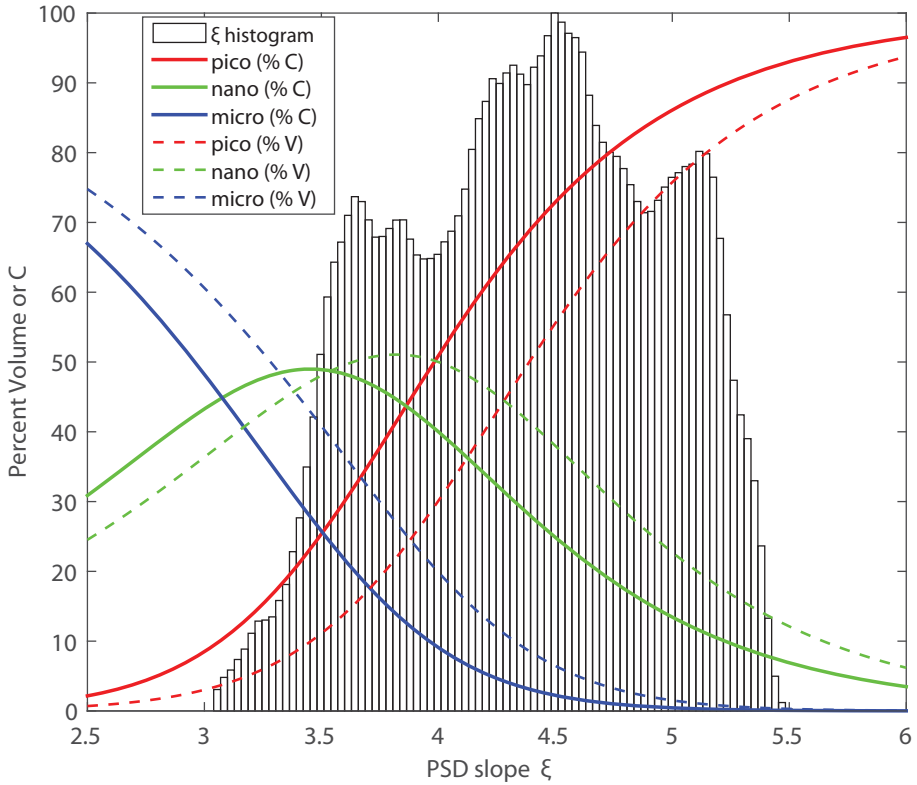

Figure 9. Fractional contribution of the three PSCs, picoplankton (red), nanoplankton (green) and microplankton (blue), to total phytoplankton carbon biomass (solid lines) and to total biovolume concentration (dashed lines), as functions of the PSD slope ξ. Limits of integration are the operational limits as indicated in Figs. 5 and 7 and Sect. 2.1.2. Also shown is the histogram of PSD slopes ξ from the mapped image of SeaWiFS mission climatology (September 1997–December 2010), normalized to the highest count bin.

OSD
12, 573–644, 2015

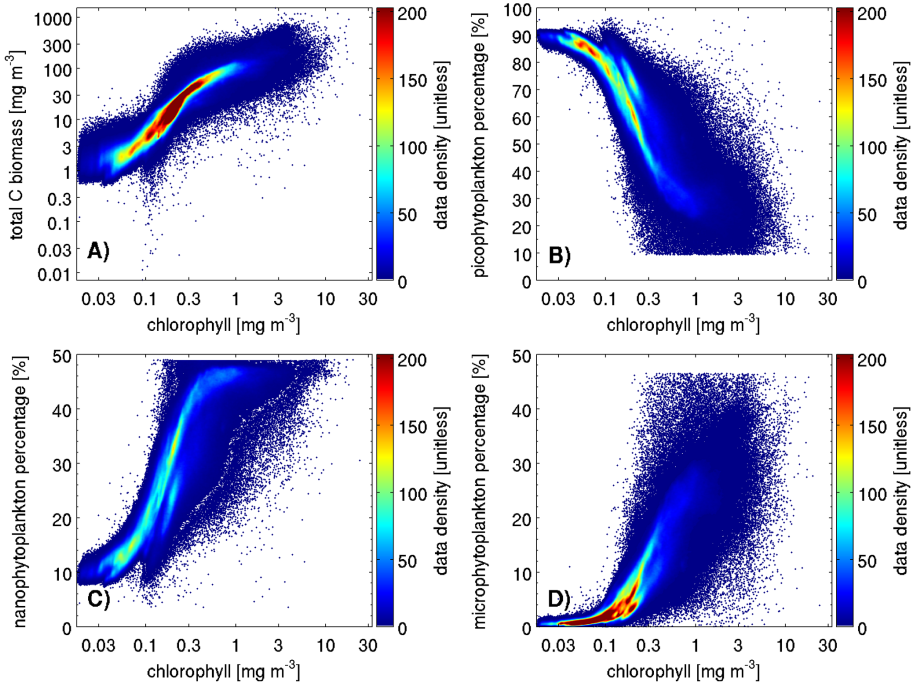

Figure 10. Smoothed bivariate histograms of chlorophyll concentration and **(a)** total phytoplankton C biomass, **(b)** picoplankton, **(c)** nanoplankton and **(d)** microplankton fractional contributions to the total algal C biomass. The histograms were computed from the global mission composite of standard mapped SeaWiFS observations (September 1997–December 2010). The colors indicate the number of pixels that fall into each bivariate bin. The counts are shown in linear space, whereas the bins themselves are in logarithmic space. Data from continental shelf regions (< 200 m) are excluded.

OSD
12, 573–644, 2015

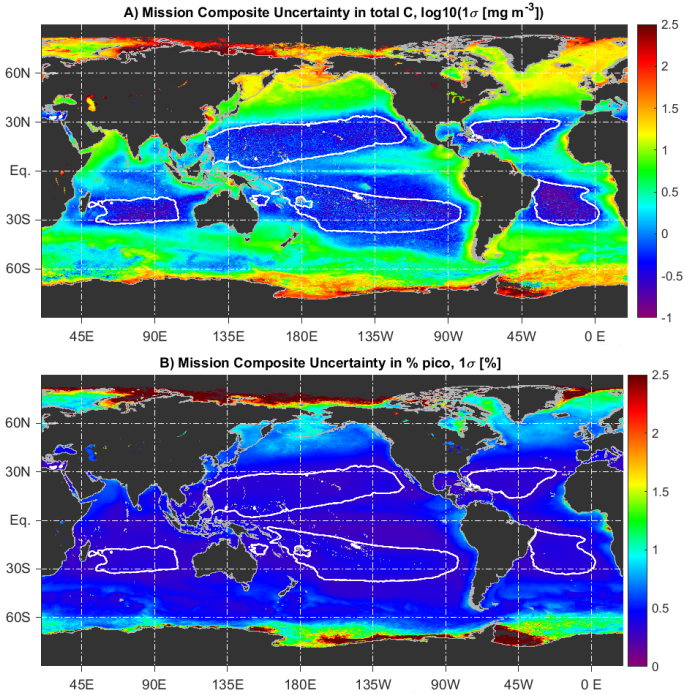

Figure 11. (a) Propagated uncertainty in the mission mean of total phytoplankton carbon concentration (one standard deviation in mg C m^{-3}, shown in log10 space). This is a partial uncertainty estimate due to the quantifiable PSD parameter uncertainties and the uncertainties of the allometric coefficients. Uncertainties are propagated to the individual monthly images using Eq. (6) and composite imagery uncertainty (which is reduced due to averaging) is estimated using Eq. (7). (Sect. 2.5). **(b)** As in **(a)**, but for the mission mean of percent picoplankton contribution to carbon biomass (one standard deviation in percent).

OSD
12, 573–644, 2015

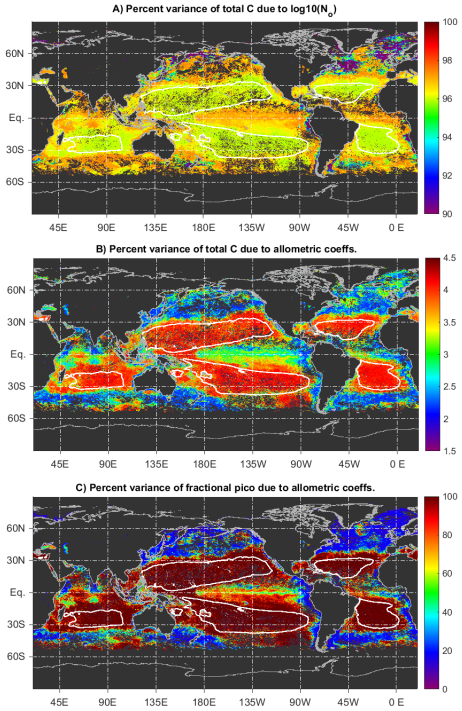

Figure 12. Fraction of uncertainty of total phytoplankton carbon biomass due to **(a)** the N_o PSD parameter, and **(b)** the allometric coefficients. The percent of total variance is shown. The third quantified source of uncertainty, the PSD slope ξ, contributes negligible amounts of variance (< 5 % for most pixels) and is not shown (the three sources add up to a total of 100 % at each pixel). May of 2004 is shown as an example. **(c)** The fraction of propagated variance of percent C-based picoplankton due to the allometric coefficients; the remainder to 100 % is due to the PSD slope ξ.

OSD
12, 573–644, 2015

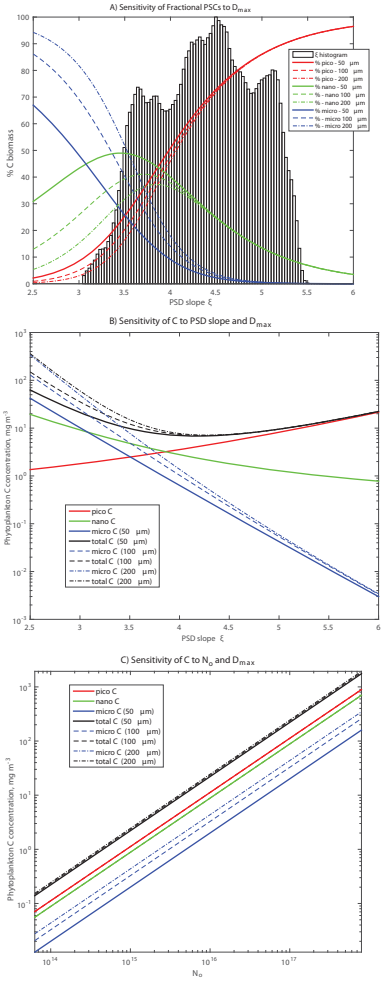

OSD
12, 573–644, 2015

Carbon-based phytoplankton size classes retrieved via the PSD

T. S. Kostadinov et al.

Figure 13. Sensitivity analyses of total and partitioned phytoplankton C biomass to the maximum limit of integration, D_{max} (Eq. 4), and the PSD parameters ξ and N_o: **(a)** the three PSCs defined as percent contributing to total C biomass, as a function of PSD slope ξ, for three different values of D_{max}, as indicated. The histogram of the mission composite PSD slope image is included (normalized to the highest count bin); **(b)** Total and partitioned absolute phytoplankton carbon concentration as a function of the PSD slope ξ, when N_o is fixed at $15.5\,m^{-4}$; **(c)** Total and partitioned absolute phytoplankton carbon concentration as a function of N_o, when the PSD slope is fixed at $\xi = 4$. In panels **(b)** and **(c)**, the effect of varying D_{max} on total and microplankton C is also shown, as indicated. The cases corresponding to the operational value ($D_{max} = 50\,\mu m$) are plotted in bold solid lines in all three panels.

OSD
12, 573–644, 2015

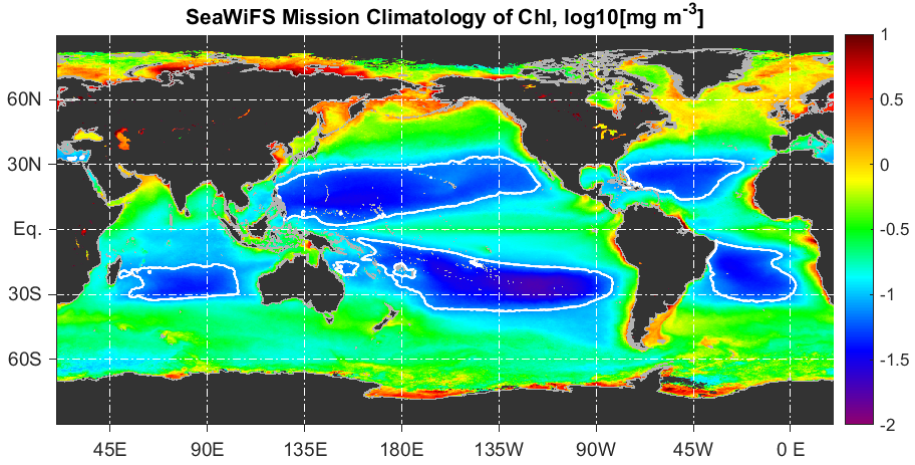

Figure A1. SeaWiFS mission composite (September 1997–December 2010) of chlorophyll (Chl) concentration [mg m^{-3}], using the standard SeaWiFS algorithm OC4v6.

OSD
12, 573–644, 2015

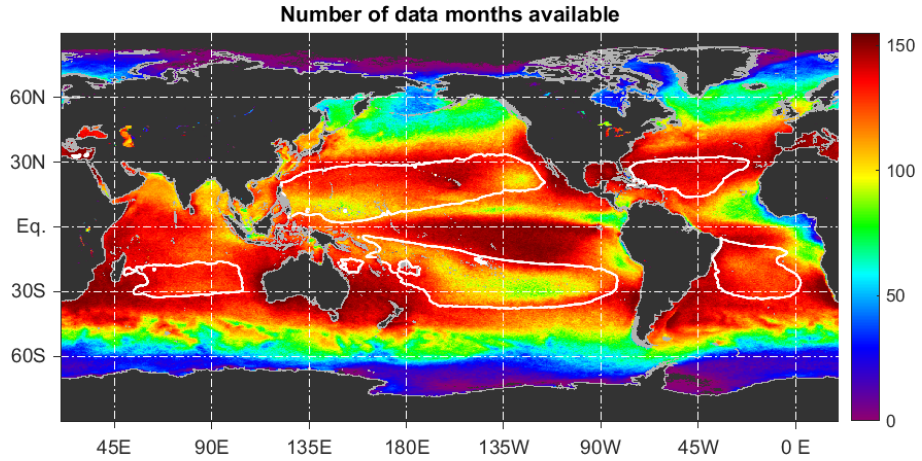

Figure A2. The number of data values contributing to the SeaWiFS mission composite means of the carbon-based products. The number of available monthly data files for the SeaWiFS mission is 157, but the maximum of available data points at any pixel as indicated here is $N = 155$, reflecting several months with very sparse data in the latest few SeaWIFS years, due to data outages.

OSD
12, 573–644, 2015